iScience

Article

Designer polyQ fusion proteins sequester USP7/HDM2 for modulating P53 functionality

Graphical abstract

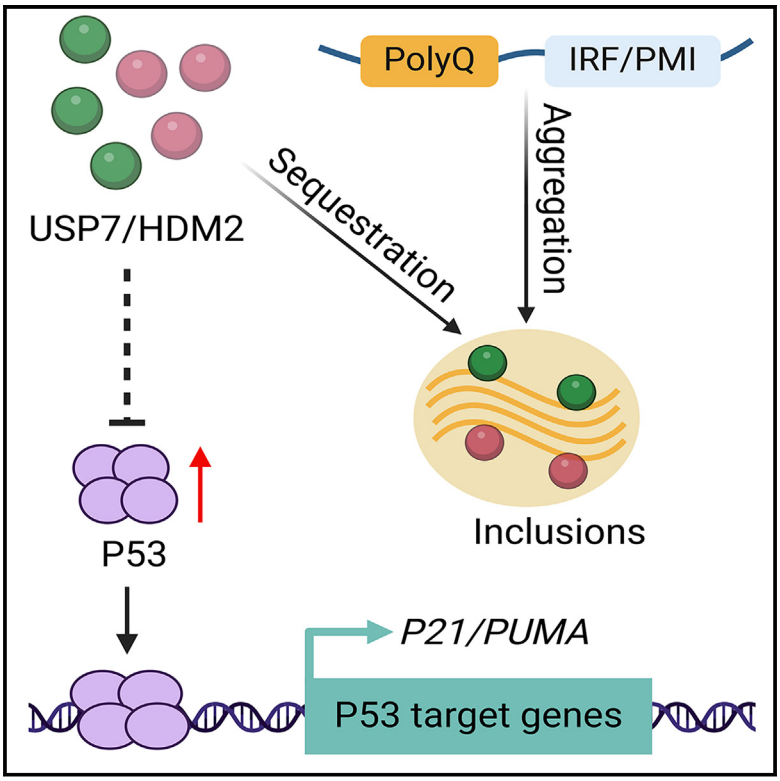

Highlights

- PolyQ fusions were engineered by combination of polyQ and target-binding sequences
- The designer polyQ fusions sequester USP7/HDM2 for modulating P53 functionality
- These sequestration effects up-regulate the expression of P53 downstream genes
- This polyQ-fusion strategy provides a therapeutic potential for diseases

Authors

Xiang-Le Zhang, Hong-Wei Yue, Ya-Jun Liu, ..., Yin-Hu Liu, Lei-Lei Jiang, Hong-Yu Hu

Correspondence

hyhu@sibcb.ac.cn

In brief

Biochemistry; Protein structure aspects; Cancer

Zhang et al., 2025, iScience *28*, 112025
March 21, 2025
https://doi.org/10.1016/j.isci.2025.112025

CellPress

iScience

CellPress
OPEN ACCESS

Article

Designer polyQ fusion proteins sequester USP7/HDM2 for modulating P53 functionality

Xiang-Le Zhang,[1,2] Hong-Wei Yue,[1,2] Ya-Jun Liu,[1,2] Jian-Yang Wang,[1,2] Heng-Tong Duan,[1,2] Yin-Hu Liu,[1,2] Lei-Lei Jiang,[1] and Hong-Yu Hu[1,3,*]

[1]Key Laboratory of RNA Innovation, Science and Engineering, Shanghai Institute of Biochemistry and Cell Biology, Center for Excellence in Molecular Cell Science, Chinese Academy of Sciences, Shanghai 200031, P.R. China

[2]University of Chinese Academy of Sciences, Beijing 100049, P.R. China

[3]Lead contact

*Correspondence: hyhu@sibcb.ac.cn

https://doi.org/10.1016/j.isci.2025.112025

SUMMARY

Overexpression of USP7 and HDM2 inactivates P53 signaling in tumor cells and facilitates their progression, but suppression of these targets by conventional strategies to reactivate P53 function remains a challenge. We applied polyQ sequences and target-interacting peptides to engineer polyQ fusion proteins that specifically sequester the targets, hence depleting their availabilities and modulating the P53 functionality. We have revealed that the designer fusion $Atx7_{93Q}$-N172-IRF (IRF sequence: SPGEGPSGTG) sequesters USP7 and/or HDM2 into aggregates and thereby increases the P53 level, but it depends on the IRF repeats fused, suggesting that depletion of the USP7 availability plays a dual role in controlling P53 stability. Direct sequestration of HDM2 by $Atx7_{93Q}$-N172-PMI (PMI: TSFAEYWNLLSP) remarkably reduces the protein level of soluble HDM2 and hence increases the P53 level, which consequently up-regulates expression of the downstream genes. The polyQ-fusion strategy is feasible to modulate the P53 stability and functionality, furnishing a therapeutic potential for cancers.

INTRODUCTION

Protein aggregation is a common biological process where improperly processed or misfolded proteins tend to form aggregates accumulating within cells.[1,2] This phenomenon is often observed in various neurodegenerative diseases, especially in polyglutamine (polyQ) diseases, which are caused by the unstable expansion of *CAG* trinucleotide repeats in specific gene sequences.[3] Research also indicates that protein aggregation might serve a protective role by segregating misfolded or damaged proteins, thus potentially safeguarding cellular functions.[4–6] During the aggregation process, polyQ-expanded (PQE) proteins can effectively sequester cellular components into aggregates through their own structural domains/motifs,[7–9] ubiquitin-mediated interaction,[10–12] or RNA-mediated interaction.[13,14] This may lead to reduced solubility and availability of the sequestered biomolecules essential to cellular homeostasis, potentially impairing their biological functions and consequently altering the cell fates.[15,16]

The polyQ tract is an aggregation-prone sequence, whereas polyQ expansion can enhance aggregate formation and maturation,[17] but it is somehow relatively inert or even protective to the cells. Based on these biochemical properties, we designed a series of chimeric proteins, combining a polyQ tract with one or more peptide sequences specifically interacting with the target proteins (enzymes). The designer polyQ fusion can sequester the target proteins into aggregates to reduce their cellular availabilities and modulate their functionalities. In this study, we took USP7-HDM2-P53 axis as an example and designed several polyQ fusion proteins to sequester USP7 and/or HDM2 and modulate the stability and functionality of the P53 protein.

Approximately two-thirds of human tumors are linked to P53 inhibition and its intracellular degradation. The stability of the tumor suppressor protein P53 is significantly influenced by the combined actions of ubiquitin-specific protease 7 (USP7), mouse/human double minute 2 homolog (MDM2/HDM2), and murine/human double minute X (MDMX/HDMX).[18,19] USP7, also named as herpesvirus-associated ubiquitin-specific protease (HAUSP), has been associated with various cancers. It can indirectly facilitate P53 degradation by stabilizing HDM2, which serves as an E3 ligase for P53 ubiquitination.[20–22] Additionally, USP7 has the ability to directly bind to and stabilize P53 through its deubiquitinating activity.[23] In this regard, overexpression of HDM2 or inactivation of USP7 will alleviate the tumor-suppressing capacity of P53 and facilitate tumor cell survival.[22,24] Consequently, antagonizing both USP7 and HDM2 to stabilize and activate P53 might be a feasible strategy for antitumor drug design.[25–28]

Our results demonstrate that the polyQ fusions can effectively sequester USP7 into aggregates or inclusions and thus reduce the availability of USP7, which plays a dual role in controlling P53 stability but perhaps due to the functional redundancy of USP7 in cancer cells.[29] Additionally, depletion of soluble HDM2 can reduce the ubiquitination level of P53 and up-regulate

expression of the downstream genes in the USP7-HDM2-P53 pathway. This study develops a polyQ-fusion strategy to modulate cell functions and may also provide a therapeutic potential for diverse diseases.

RESULTS

Design of the polyQ fusion proteins for specifically sequestering USP7

As known, protein aggregation can sequester cellular essential factors into aggregates or inclusions through their interacting domains or motifs and consequently impair the biological functions of targeted proteins.[16] To specifically sequester cellular target proteins (enzymes) and suppress their functions, we designed and constructed a series of fusion proteins, based on an amyloidogenic core (e.g., polyQ tract) and an interacting peptide sequence, to modulate the biological functions of these indicated targets (Figure 1A). Because the target protein USP7 is a nuclear protein, a nuclear localization signal (NLS) is required for directing the fusion protein into the nucleus. It was previously reported that viral interferon regulatory factor 1 (vIRF1) specifically interacts with USP7 via a peptide sequence of SPGEGPSGTG.[30] Thus, we applied this sequence, hereinafter referred to as IRF, to fuse with the polyQ tract to construct a polyQ fusion protein.

First, we selected the N-terminal fragments of PQE huntingtin (Htt) and ataxin-7 (Atx7),[10,11] namely Htt-N171 and Atx7-N172, respectively, to serve as amyloidogenic cores in our polyQ fusion proteins (Figures 1A and S1A). We co-transfected FLAG-tagged NLS-Atx7$_{10Q}$-N172, NLS-Htt$_{18Q}$-N171, or their respective fusions (IRF or 3IRF) with HA-tagged USP7 into HEK 293T cells and performed co-immunoprecipitation (co-IP) experiment to characterize their interactions. The data showed that only the fusion proteins containing the IRF sequence could interact with USP7, whereas the Atx7$_{10Q}$-N172 and Htt$_{18Q}$-N171 without IRF fusion did not interact with USP7 (Figures 1B and S1B), suggesting that the polyQ fusion proteins specifically interact with USP7 via their fused IRF sequence. Subsequently, we performed supernatant/pellet (S/P) fractionation, and the result indicated that Atx7$_{93Q}$-N172-IRF/3IRF could precipitate more exogenous USP7 into the pellet fraction than the non-peptide fusion form (Figure 1C). However, there was no significant difference in the USP7 level precipitated by Htt$_{100Q}$-N171-IRF as compared with Htt$_{100Q}$-N171 (Figure S1C), possibly because the free Htt$_{100Q}$-N171 fragment formed amorphous aggregates with different sizes and could precipitate USP7 into pellet with a non-specific manner. Therefore, we consider Atx7$_{93Q}$-N172 as an amyloidogenic core suitable for fusing an interacting peptide to specifically sequester USP7 into aggregates in cells.

Sequestration of endogenous USP7 into aggregates by polyQ-IRF fusions

Since USP7 is shown overexpressing in various cancer phenotypes, disrupting its biological function has become a promising strategy in oncological research for cancer therapy.[31,32] To target the endogenous USP7 by designer polyQ-IRF fusions, we overexpressed these fusion proteins in A549 cells and initially assessed their impact on the USP7 levels. The result exhibited that the protein levels of endogenous USP7 were almost equivalent upon overexpression of Atx7$_{93Q}$-N172 and its IRF/3IRF fusion forms (Figure 2A), indicating that overexpression of polyQ-IRF fusions did not alter the cellular total USP7 levels. S/P fractionation showed that overexpression of Atx7$_{93Q}$-N172-IRF/3IRF in A549 cells significantly decreased the USP7 level in supernatant, whereas it remarkably increased the accumulation of USP7 in pellet (Figure 2B). We also examined the sequestration capacity of exogenous USP7 by these polyQ-IRF fusions in HEK 293T cells and observed an increasing amount of the exogenous USP7 in the pellet fraction sequestered by Atx7$_{93Q}$-N172-IRF/3IRF (Figure S2A). These findings suggest that the IRF or 3IRF fusion form can substantially reduce the solubility and perhaps availability of USP7 within cells without altering its total expression level.

Subsequently, we conducted immunofluorescence imaging for visualizing co-localization and sequestration in both A549 (Figure 2C) and HEK 293T (Figures S2B and S2C) cells. Although Atx7$_{93Q}$-N172 formed large puncta in nucleus, it did not co-localize with USP7, indicating that the Atx7$_{93Q}$-N172 without IRF fusion could not sequester endogenous USP7 into the inclusions. However, the inclusions formed by Atx7$_{93Q}$-N172-IRF/3IRF exhibited evident co-localization with the endogenous USP7 (Figures 2C and S2B). It means that Atx7$_{93Q}$-N172-IRF/3IRF can induce endogenous USP7 to accumulate in the large ring-like puncta. Note that each punctum may contain a solid and condensed core of protein aggregates, which cannot be stained by the dyes, so it looks like a hollow ring under microscopic imaging. Similar result was also obtained from the co-localization of exogenous USP7 with the inclusions formed by Atx7$_{93Q}$-N172-IRF/3IRF in HEK 293T cells (Figure S2C). Therefore, we conclude that the polyQ-IRF fusions can effectively sequester USP7 into aggregates or inclusions in cells through their combined IRF peptide sequences, which may reduce the solubility and availability of USP7 and interfere with its biological function in the cellular environment.

Accumulation of endogenous HDM2 with USP7 by polyQ-IRF fusions

USP7 plays a critical role in cellular processes; it interacts with HDM2 and enhances its stability through the deubiquitination pathway.[33,34] Considering the interaction between USP7 and HDM2, we further examined whether the polyQ-IRF fusions could sequester endogenous HDM2 together with USP7. Our S/P fractionation data indicated that, upon overexpression of Atx7$_{93Q}$-N172-IRF/3IRF in A549 cells, there was a significant increase of the amount of HDM2 in the pellet fraction but no change observed in the supernatant (Figure 3A). Immunofluorescence imaging also showed that the endogenous HDM2 was co-localized with the puncta formed by Atx7$_{93Q}$-N172-IRF/3IRF (Figure 3B), but there was no such co-localization observed between Atx7$_{93Q}$-N172 and HDM2. This observation was also obtained from the exogenous HDM2 co-localized with the puncta formed by Atx7$_{93Q}$-N172-IRF/3IRF in HEK 293T cells (Figure S3). These data suggest that the polyQ-IRF fusions can also accumulate HDM2 via sequestering USP7 into aggregates.

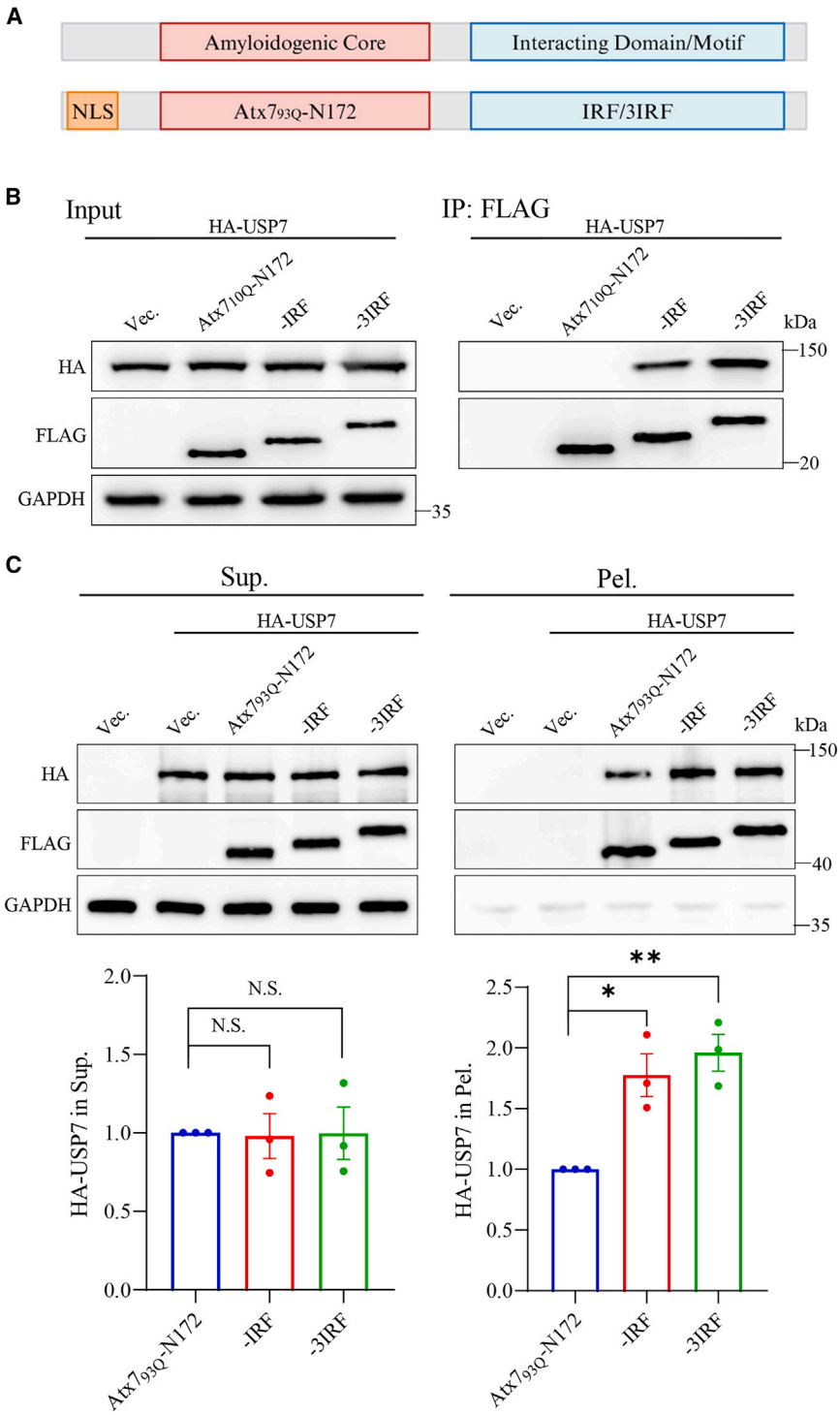

Figure 1. The N-terminal fragment of PQE Atx7 as an aggregation template for designing polyQ fusion proteins

(A) Schematic diagram of the designer polyQ-fusion proteins based on Atx7$_{93Q}$-N172. Atx7$_{93Q}$-N172, the N-terminal 172-residue fragment of Atx7$_{93Q}$; NLS, nuclear localization signal; IRF, a homologous sequence of vIRF, SPGEGPSGTG; 3IRF, triplicate of IRF.

(B) Examining the interaction between polyQ-IRF fusion and USP7 by co-IP assay. HEK 293T cells were co-transfected with FLAG-tagged NLS-Atx7$_{10Q}$-N172 or its IRF/3IRF fusion and HA-USP7, and 48 h post-transfection, the cell lysates were subjected to co-IP assay with anti-FLAG agarose beads. Vec., vector; Atx7$_{10Q}$-N172, tagged with an NLS sequence; IRF, NLS-Atx7$_{10Q}$-N172-IRF; 3IRF, NLS-Atx7$_{10Q}$-N172-3IRF.

(C) S/P fractionation for characterizing the distribution of exogenous USP7 in supernatant and pellet. HEK 293T cells were co-transfected with FLAG-tagged NLS-Atx7$_{93Q}$-N172 or its IRF/3IRF fusion and HA-USP7, and after cultured for 48 h, the USP7 levels in the supernatant and pellet fractions were detected and analyzed. Sup., supernatant; Pel., pellet. Vec., vector; Atx7$_{93Q}$-N172, with an NLS sequence; IRF, NLS-Atx7$_{93Q}$-N172-IRF; 3IRF, NLS-Atx7$_{93Q}$-N172-3IRF. Data are shown as mean ± SD ($n = 3$). *$p < 0.01$; **$p < 0.01$; N.S., no significance. See also Figure S1.

Effects of polyQ-IRF fusions on P53 stability

The USP7-HDM2-P53 signaling pathway plays a critical role in maintaining cellular homeostasis.[35,36] Dysfunction in USP7 typically leads to accelerated degradation of HDM2 and in turn enhances the P53 stability.[37] To understand the sequestration effects of the polyQ-IRF fusions on USP7 and HDM2 that directly influence P53 stability, we overexpressed Atx7$_{93Q}$-N172-IRF/3IRF in HEK 293T cells, treated the cells with MG132, and conducted immunoprecipitation to assess P53 ubiquitination. The results showed that Atx7$_{93Q}$-N172-IRF reduced the ubiquitination level of P53 remarkably, whereas Atx7$_{93Q}$-N172-3IRF had little impact on the P53 ubiquitination (Figure S4). Subsequently, we transfected various polyQ-IRF fusion forms (Atx7$_{93Q}$-N172-IRF, 2IRF, or 3IRF) in A549 cells and detected the P53 levels. The data showed that Atx7$_{93Q}$-N172 did not alter the P53 level, whereas Atx7$_{93Q}$-N172-IRF/2IRF led to a significant increase in the P53 levels (Figure 4A). Intriguingly, overexpression of Atx7$_{93Q}$-N172-3IRF caused no significant changes in the P53 level compared to Atx7$_{93Q}$-N172, being consistent with the above-mentioned observation that overexpression of Atx7$_{93Q}$-N172-3IRF did not alter P53 ubiquitination considerably.

To further verify whether the changes in P53 stability were caused by sequestration of USP7 and HDM2, we conducted dose-dependent experiments to analyze the effects of the polyQ-IRF fusions on P53 stability. The results showed that the P53 level in cells increased with the transfected plasmid dose of Atx7$_{93Q}$-N172-IRF/2IRF

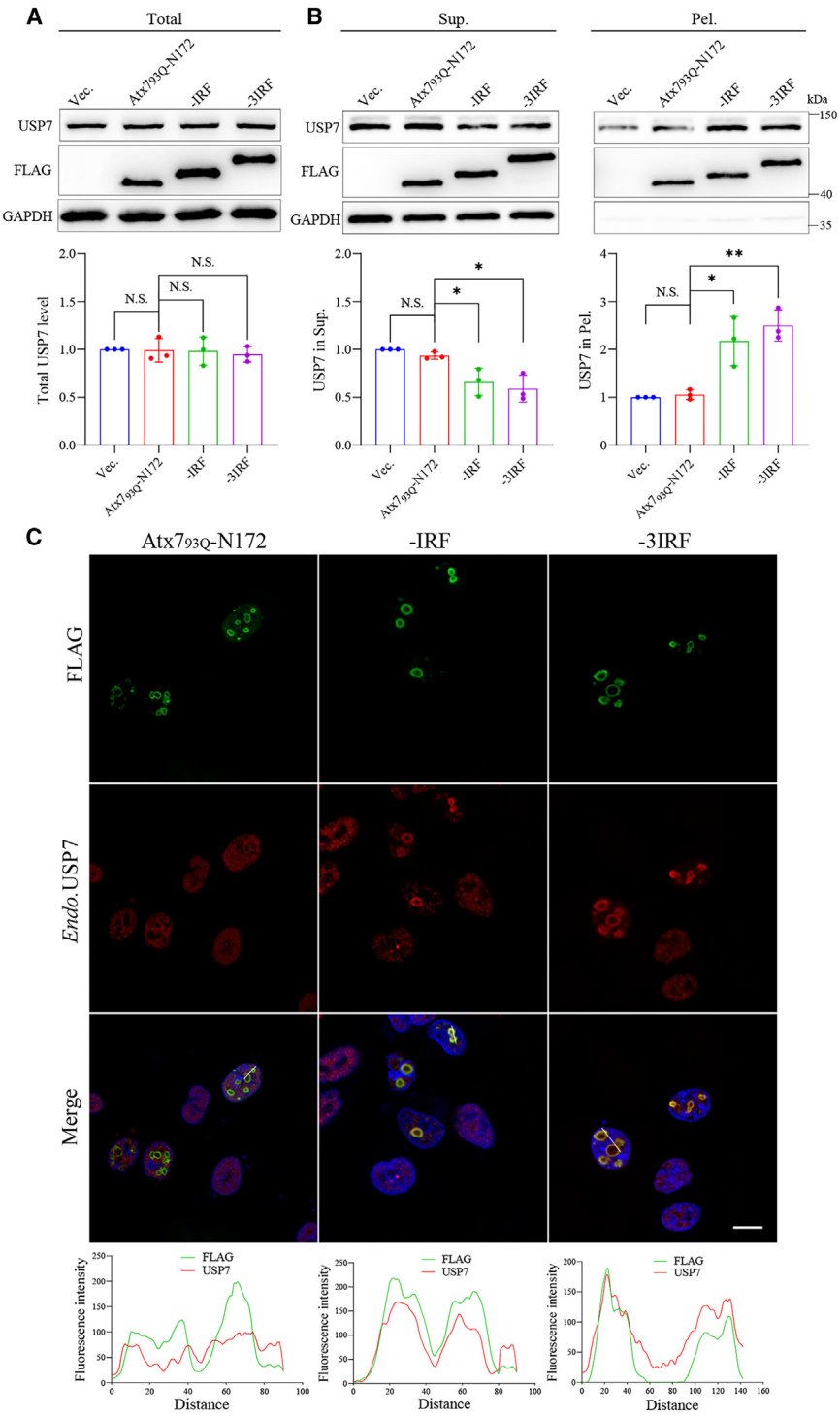

Figure 2. Sequestration of endogenous USP7 by polyQ-IRF fusions

(A) Detection of the total USP7 levels in A549 cells. A549 cells were transfected with FLAG-tagged NLS-Atx7$_{93Q}$-N172 or its IRF/3IRF fusion, and after cultured for 48 h, the total USP7 levels were detected and analyzed. Vec., vector; Atx7$_{93Q}$-N172, with an NLS sequence; IRF, NLS-Atx7$_{93Q}$-N172-IRF; 3IRF, NLS-Atx7$_{93Q}$-N172-3IRF.

(B) S/P fractionation for characterizing the distribution of endogenous USP7 in supernatant and pellet. A549 cells were transfected with FLAG-tagged NLS-Atx7$_{93Q}$-N172 or its IRF/3IRF fusion, and after 48-h culture, the USP7 levels in the supernatant and pellet fractions were detected and analyzed. Sup., supernatant; Pel., pellet. Data are shown as mean ± SD (n = 3). *p < 0.05; **p < 0.01; N.S., no significance.

(C) Immunofluorescence imaging for characterizing the co-localization of endogenous USP7 with the aggregates formed by Atx7$_{93Q}$-N172 or its IRF/3IRF fusion. A549 cells were transfected with FLAG-tagged NLS-Atx7$_{93Q}$-N172 or its IRF/3IRF fusion, and after cultured for 48 h, the cells were fixed and immunostained with anti-FLAG (green) and anti-USP7 (red) antibodies. Nuclei were stained with Hoechst (blue). Scale bar, 10 μm. *Bottom*: co-localization analysis of the fluorescence signals for the distance represented by white lines. See also Figure S2.

(Figures 4B and 4C). It was likely that the P53 level tended to reach a saturation upon transfection of Atx7$_{93Q}$-N172-2IRF with 0.8 μg of the plasmid, whereas it did not get saturation within the experimental dose of Atx7$_{93Q}$-N172-IRF. Unexpectedly, the P53 level was decreased slightly with the increasing dose of Atx7$_{93Q}$-N172-3IRF (Figure 4D). Considering the dual regulatory function of USP7 in P53 stability, we speculate that, with the increasing number of IRF repeats, the polyQ fusion may deplete more USP7 from the soluble fraction, leading to attenuate its deubiquitination function on P53 and thereby reduce the P53 level.

PolyQ-IRF fusions dually modulate P53 signaling by sequestering USP7/HDM2

P53, a pivotal tumor suppressor protein, orchestrates many cellular processes, including DNA repair, cell-cycle arrest, and apoptosis.[38–40] Since the 3IRF fusion form had an opposite regulatory effect on the P53 level compared to the others, we assessed the expression levels of P53 downstream genes (*PUMA* and *P21*) in the A549 cells overexpressing Atx7$_{93Q}$-N172-IRF/3IRF fusions, respectively. The data showed that overexpression of Atx7$_{93Q}$-N172-IRF significantly increased the protein levels of PUMA (Figure 5A) and P21 (Figure 5B), whereas Atx7$_{93Q}$-N172-3IRF had only little effects on the proteins. These are consistent with our previous results that the IRF and 3IRF forms exert opposite effects on the P53

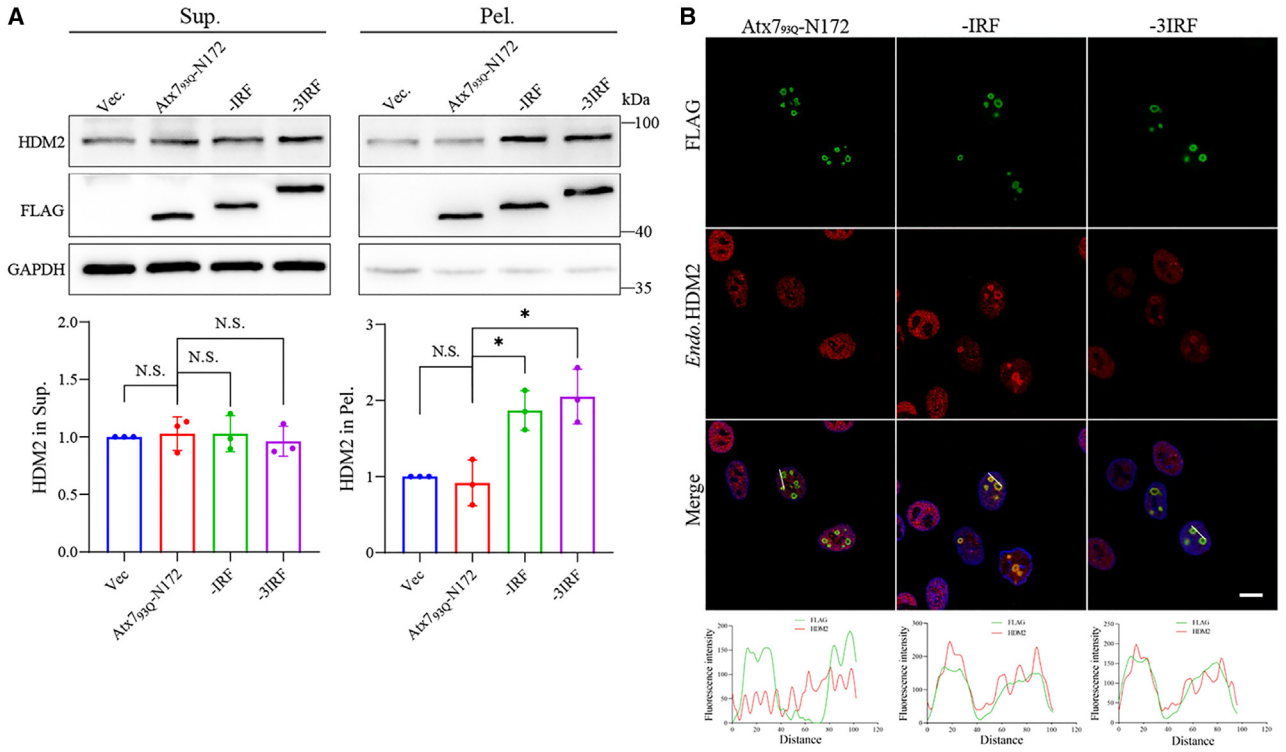

Figure 3. Sequestration of endogenous HDM2 by polyQ-IRF fusions

(A) S/P fractionation for characterizing the distribution of HDM2 in supernatant and pellet. A549 cells were transfected with FLAG-tagged NLS-Atx7$_{93Q}$-N172 or its IRF/3IRF fusion, and after cultured for 48 h, the HDM2 levels in supernatant and pellet were detected and analyzed. Vec., vector; Atx7$_{93Q}$-N172, with an NLS sequence; IRF, NLS-Atx7$_{93Q}$-N172-IRF; 3IRF, NLS-Atx7$_{93Q}$-N172-3IRF. Data are shown as mean ± SD (n = 3). *p < 0.05; N.S., no significance.

(B) Immunofluorescence imaging for characterizing the co-localization of endogenous HDM2 with the aggregates formed by NLS-Atx7$_{93Q}$-N172 or its IRF/3IRF fusion. A549 cells were transfected with FLAG-tagged NLS-Atx7$_{93Q}$-N172 or its IRF/3IRF fusion, and after 48-h culture, the cells were fixed and immunostained with anti-FLAG (green) and anti-MDM2 (red) antibodies. Nuclei were stained with Hoechst (blue). Scale bar, 10 μm. *Bottom*: co-localization analysis of the fluorescence signals for the distance represented by white lines. See also Figure S3.

stabilities, that is, Atx7$_{93Q}$-N172-IRF can promote P53 stability and thereby activate P53 signaling, whereas Atx7$_{93Q}$-N172-3IRF cannot.

Sequestration of endogenous HDM2 into aggregates by polyQ-PMI fusions

P53 directly interacts with HDM2 (MDM2) through its N-terminal motif.[41] Based on the interacting region in P53, a modified peptide named PMI (for P53/MDM2 inhibitor; TSFAEYWNLLSP) was developed, which binds to HDM2 with a higher affinity than the homologous peptide from P53.[42,43] Thus, we constructed two polyQ-PMI fusion proteins by combining the PMI sequence with Atx7$_{93Q}$-N172 (Figure 6A) and examined whether they could sequester HDM2 into aggregates. Firstly, the co-IP data showed that Atx7$_{10Q}$-N172-PMI/3PMI interacted with HDM2 through the fused PMI sequence (Figure 6B), whereas the Atx7$_{10Q}$-N172 without PMI fusion could not. Subsequently, we overexpressed these polyQ-PMI fusions in A549 cells (Figure 6C) or HEK 293T cells (Figure S5A) and assessed the total HDM2 levels. The expression levels of endogenous HDM2 are almost equivalent upon overexpression of Atx7$_{93Q}$-N172 or its PMI/3PMI fusion form (Figure 6C), suggesting that these polyQ-PMI fusions did not alter the HDM2 levels in cells.

We then performed S/P fractionation experiments to determine the distribution of HDM2 upon overexpression of polyQ-PMI in A549 cells (Figure 6D) and HEK 293T cells (Figure S5B), respectively. The data indicated that overexpression of Atx7$_{93Q}$-N172-PMI/3PMI significantly increased the HDM2 level in pellet. Specially, the HDM2 level in supernatant remained roughly unchanged (Figure 6D) or slightly decreased in HEK 293T cells (Figure S5B). Similarly, we also observed a significant increase of the exogenous HDM2 level upon overexpression of Atx7$_{93Q}$-N172-PMI/3PMI (Figure S6A).

Immunofluorescence imaging also exhibited that all the Atx7$_{93Q}$-N172 fusions formed large nuclear puncta of inclusion bodies, whereas the inclusions formed by Atx7$_{93Q}$-N172-PMI/3PMI could co-localize with the endogenous HDM2 in both A549 cells (Figure 6E) and HEK 293T cells (Figure S5C) or with the exogenous HDM2 in HEK 293T cells (Figure S6B). Together, these results demonstrate that the designed polyQ-PMI fusions are capable of sequestering HDM2 into aggregates or inclusions,

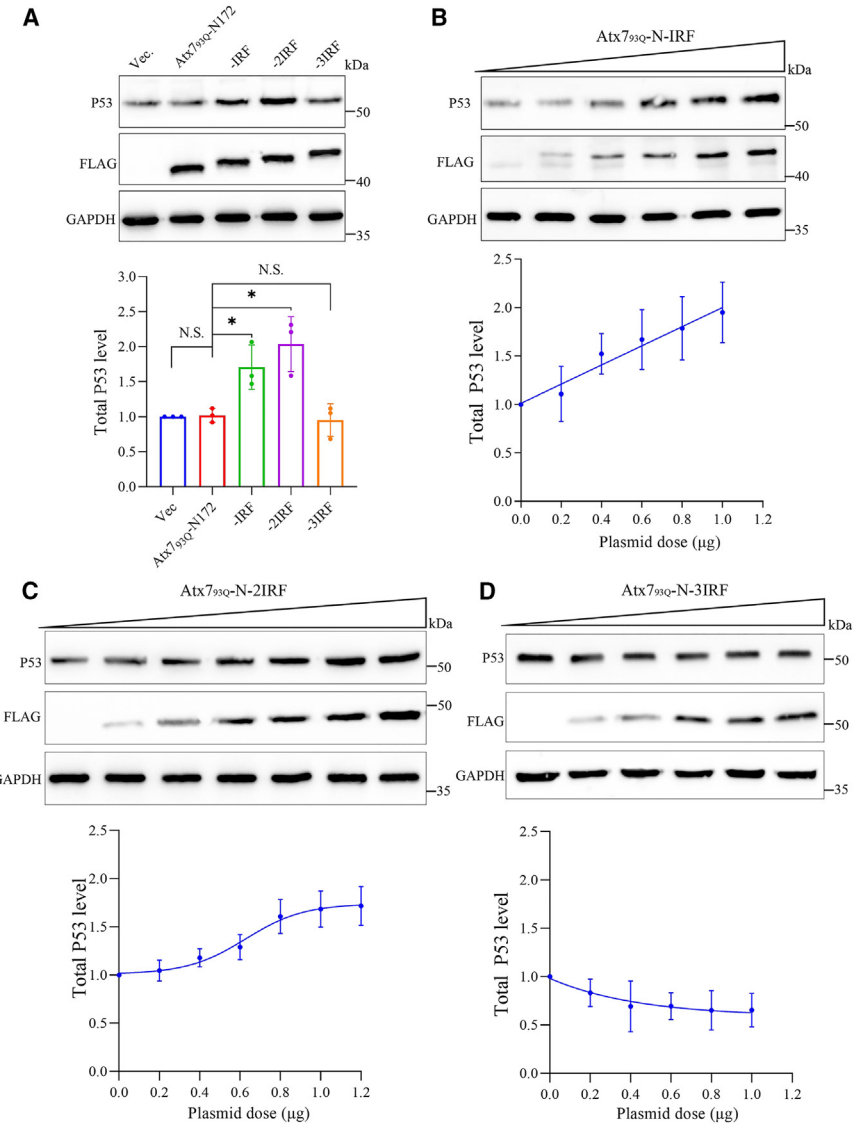

Figure 4. Effects of polyQ-IRF fusions on P53 stability

(A) Detection of the total P53 levels in A549 cells. A549 cells were transfected with FLAG-tagged NLS-Atx7$_{93Q}$-N172 or its IRF/2IRF/3IRF fusion, and 48 h post-transfection, the cell lysates were detected and analyzed. Sup., supernatant; Pel., pellet. Vec., vector; Atx7$_{93Q}$-N172, with an NLS sequence; IRF, NLS-Atx7$_{93Q}$-N172-IRF; 2IRF, NLS-Atx7$_{93Q}$-N172-2IRF; 3IRF, NLS-Atx7$_{93Q}$-N172-3IRF. Data are shown as mean ± SD (n = 3). *p < 0.05; N.S., no significance.

(B) Dose-dependent experiment for characterizing the effect of Atx7$_{93Q}$-N172-IRF fusion on the P53 level.

(C) As in (B), Atx7$_{93Q}$-N172-2IRF.

(D) As in (B), Atx7$_{93Q}$-N172-3IRF. A549 cells were transfected with indicated dose of each plasmid, and then the P53 levels were detected and analyzed. See also Figure S4.

which may consequently modulate the P53 stability and the downstream gene expression.

Sequestration of HDM2 by polyQ-PMI fusions suppresses P53 ubiquitination and hence enhances P53 stability

HDM2 serves as a negative regulator for P53; it can facilitate P53 degradation through the ubiquitin-proteasome pathway.[22,44] We have demonstrated that the polyQ-PMI fusions can specifically sequester endogenous HDM2 into aggregates in cells. To further substantiate that the HDM2 sequestration suppresses ubiquitination function of HDM2 on P53, we overexpressed these polyQ-PMI fusions in HEK 293T cells, treated the cells with MG132, and subsequently detected the ubiquitination level of P53. The data showed that overexpression of Atx7$_{93Q}$-N172-PMI/3PMI led to a considerable reduction in the ubiquitination level of P53 (Figures 7A and S7), indicating that the ubiquitination function of HDM2 was suppressed by the polyQ-PMI fusions.

To confirm the effect of HDM2 inhibition on the P53 stability, we employed siRNA to knock down the HDM2 level in A549 cells and assessed the effects of HDM2 silencing on the protein levels of P53 and its downstream target P21 (Figure S8). Indeed, silencing of HDM2 by siRNA could substantially enhance the protein level of P53 as well as P21. Subsequently, we transfected the polyQ-PMI fusions into A549 cells and detected the P53 expression levels. Similar to HDM2 silencing by siRNA, overexpression of Atx7$_{93Q}$-N172-PMI/3PMI could increase the P53 level significantly (Figure 7B). These results suggest that sequestration of endogenous HDM2 into aggregates by the polyQ-PMI fusions enhances the P53 stability effectively.

PolyQ-PMI fusions activate the P53 signaling pathway by sequestering HDM2

Given our previous finding that the polyQ-PMI fusions could enhance the P53 stability by sequestering HDM2 into aggregates, we then examined whether these fusions could activate the P53 signaling pathway. We overexpressed the polyQ-PMI fusions in A549 cells and detected the expression levels of the P53 targeted genes. The results showed that Atx7$_{93Q}$-N172-PMI/3PMI significantly up-regulated the mRNA levels of *PUMA* (Figure 8A) and *P21* (Figure 8B). In addition, we also detected the effects on their gene products and observed that Atx7$_{93Q}$-N172-PMI/3PMI could significantly increase the protein levels of both PUMA (Figure 8C) and P21 (Figure 8D), in parallel with the upregulation of P53 level by depleting the availability of HDM2. Altogether, these findings

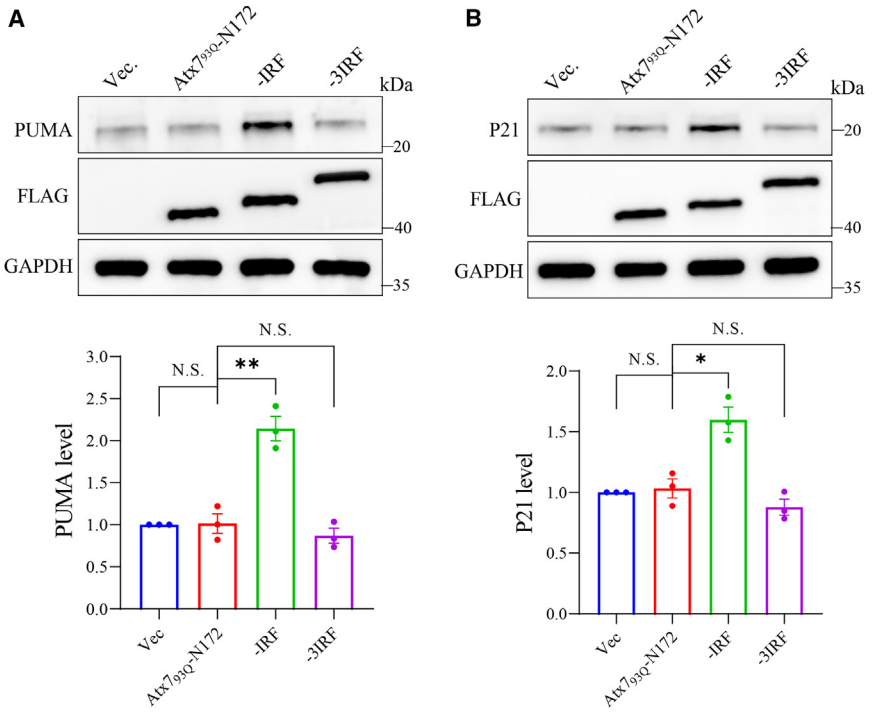

Figure 5. Detecting the protein levels of PUMA and P21 affected by polyQ-IRF fusions

(A and B) A549 cells were transfected with FLAG-tagged NLS-Atx7$_{93Q}$-N172 or its IRF/3IRF fusion, and after cultured for 48 h, the cells were lysed in RIPA buffer containing 8M urea, then the protein levels of PUMA (A) and P21 (B) were detected and analyzed. Vec., vector; Atx7$_{93Q}$-N172, with an NLS sequence; IRF, NLS-Atx7$_{93Q}$-N172-IRF; 3IRF, NLS-Atx7$_{93Q}$-N172-3IRF. Data are shown as mean ± SD (n = 3). *p < 0.05; **p < 0.01; N.S., no significance.

strongly support the viewpoint that the designer polyQ-PMI fusions activate the P53 signaling pathway by sequestering cellular HDM2.

DISCUSSION

P53 is a tumor suppressor that activates downstream target genes, such as *P21* for cell-cycle arrest, *PUMA* for apoptosis, and *BAX* to promote cell death.[45] The aberrant activities of USP7 and HDM2 suppress the normal function of P53 and thereby disrupt the natural processes of apoptosis and cell-cycle progression in cells, which may contribute to cancer initiation.[46] We have demonstrated that the designer polyQ fusion proteins can specifically sequester USP7 and/or HDM2 into aggregates or inclusions and deprive them of the functional availabilities in cells. The sequestration effect of polyQ-IRF on USP7 can attenuate the biological function of HDM2, directly reduce the ubiquitination and degradation of P53, and thereby prompt the P53 level. On the other hand, polyQ-IRF also sequesters HDM2 together with USP7 (Figure 3), which down-regulates the function of HDM2 and thus enhances the P53 stability (Figure 9). As for polyQ-PMI, it can deplete the functional availability of HDM2 by sequestering the E3 ligase directly. This sequestration effect leads to reduction of the P53 ubiquitination level and activation of the P53 signaling pathway (Figures 7 and 8), which can effectively suppress tumor progression.

Sequestration of USP7 for modulating P53 functionality

USP7 is an important target for cancer therapy. Currently, using small-molecule inhibitors or proteolysis targeting chimera (PROTAC) technique to inhibit the deubiquitination function of USP7 has become increasingly mature.[37,47] Considering that USP7 is involved in various cellular processes,[48,49] degradation of USP7 by PROTAC may lead to cellular dysfunction or even cell death.[50] Instead, polyQ fusion proteins may not influence the expression level of USP7 in cells (Figure 2); diminishing the soluble fraction of USP7 will suppress its biological availability and deubiquitination function. Thus, polyQ fusions may have lesser impact on cellular processes, which provides a substantial potential in the application of targeted therapeutic strategies. Of note, protein aggregates may exhibit substantial toxicity that is detrimental to cell function and fate. However, studies have shown that formation of aggregates can reduce intracellular toxicity by segregating the damaged proteins,[4,5] which partially alleviates the burden on the protein degradation system.[51]

Sequestration of USP7 dually modulates the P53 stability

It has been reported that the expression level of USP7 is elevated in several types of tumor cells.[31,32] Overexpression of USP7 causes deubiquitination of HDM2 and degradation of P53, which can promote tumor progression.[46] We previously proposed that protein aggregation has great impact on molecular pathways and cellular events by sequestering essential factors.[16] For example, PQE Atx2 can sequester Raptor or DDX6 into aggregates, leading to impairment of the mTORC1 signaling[52] or the processing-body homeostasis.[53] Interestingly, although the IRF or 2IRF fusion form causes an enhanced stability of P53, the 3IRF form slightly decreases the P53 level (Figure 4). We speculate that, besides the USP-HDM2-P53 axis, another pathway by which USP7 regulates the P53 stability may have also been influenced by the triplicate IRF fusion.

Alternatively, USP7 can also stabilize P53 through direct deubiquitination even in the presence of excess HDM2, inducing P53-dependent tumor cell suppression and apoptosis.[54] In this way, the loss of USP7 function may lead to an increase of P53 ubiquitination and thereby decrease of the P53 level. The 3IRF fusion form sequesters USP7 strongly, which may attenuate the deubiquitination of P53 and in turn reduce the

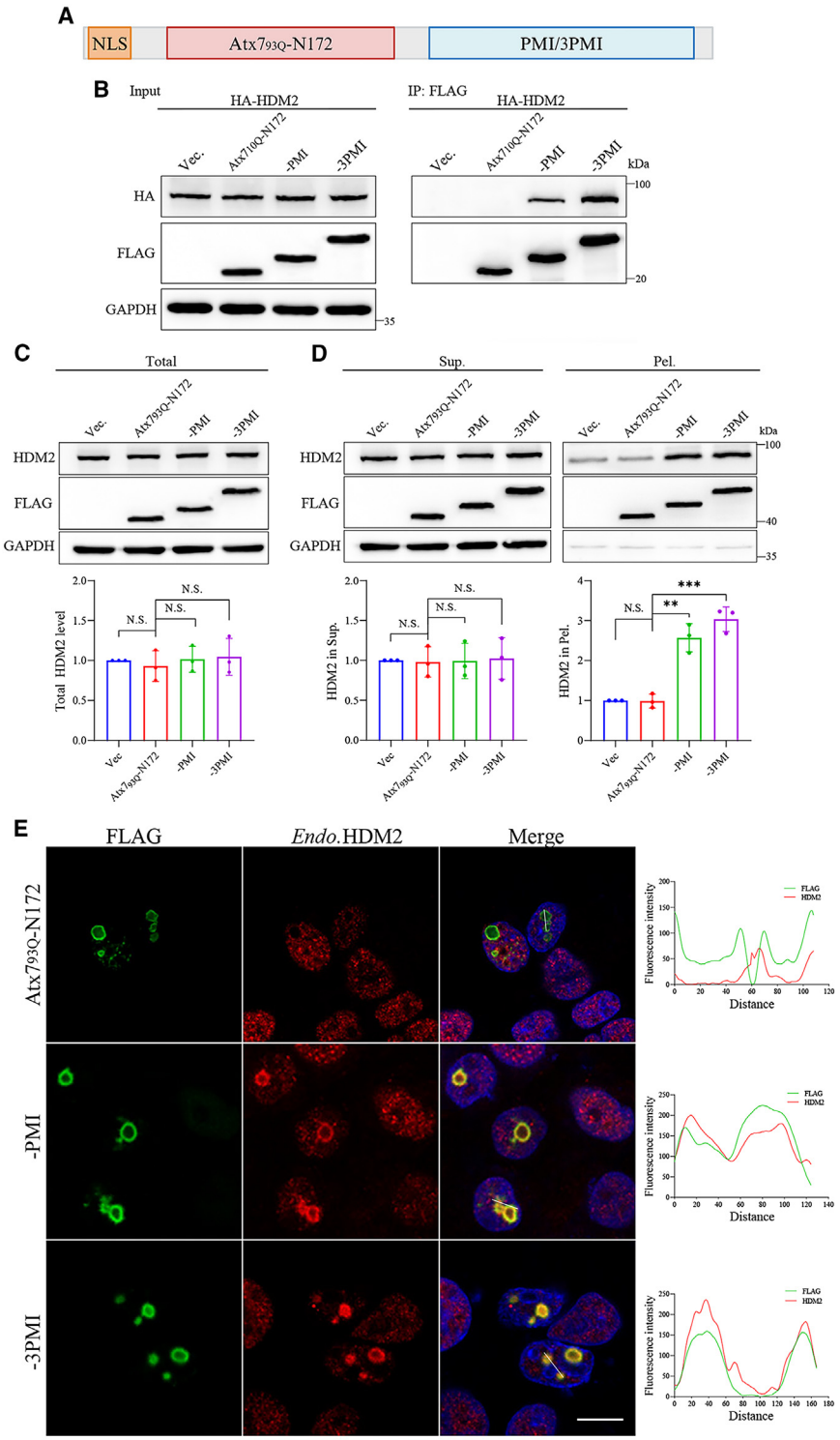

Figure 6. Sequestration of endogenous HDM2 directly by polyQ-PMI fusions

(A) Schematic diagram of polyQ-PMI fusions. Atx7$_{93Q}$-N172, the N-terminal 172-residue fragment of Atx7$_{93Q}$; NLS, nuclear localization signal; PMI, an optimized sequence based on P53: TSFAEYWNLLSP; 3PMI, triplicate of PMI.

(B) Examining the interaction of polyQ-PMI with HDM2 by co-IP assay. HEK 293T cells were co-transfected with FLAG-tagged NLS-Atx7$_{10Q}$-N172 or its PMI/3PMI fusion with HA-HDM2, and 48 h post-transfection, the cell lysates were subjected to co-IP assay with anti-FLAG agarose beads. Vec., vector; Atx7$_{10Q}$-N172, with an NLS sequence; PMI, NLS-Atx7$_{10Q}$-N172-PMI; 3PMI, NLS-Atx7$_{10Q}$-N172-3PMI.

(C) Detection of the total HDM2 levels in A549 cells. A549 cells were transfected with FLAG-tagged NLS-Atx7$_{93Q}$-N172 or its PMI/3PMI fusion, and after cultured for 48 h, the cells were lysed in RIPA buffer containing 8M urea, then the HDM2 levels were detected and analyzed. Vec., vector; Atx7$_{93Q}$-N172, with an NLS sequence; PMI, NLS-Atx7$_{93Q}$-N172-PMI; 3PMI, NLS-Atx7$_{93Q}$-N172-3PMI. Data are shown as mean ± SD (n = 3). N.S., no significance.

(D) S/P fractionation for characterizing the distribution of endogenous HDM2 in supernatant and pellet. A549 cells were transfected with FLAG-tagged NLS-Atx7$_{93Q}$-N172 or its IRF/3IRF fusion, and after cultured for 48 h, the HDM2 levels in supernatant and pellet were detected and analyzed. Sup., supernatant; Pel., pellet. Data are shown as mean ± SD (n = 3). $^{**}p < 0.01$; $^{***}p < 0.001$; N.S., no significance.

(E) Immunofluorescence imaging for characterizing the co-localization of endogenous HDM2 with the aggregates formed by Atx7$_{93Q}$-N172 or its PMI/3PMI fusion. A549 cells were transfected with FLAG-tagged NLS-Atx7$_{93Q}$-N172 or its PMI/3PMI fusion, and after cultured for 48 h, the cells were fixed and immunostained with anti-FLAG (green) and anti-MDM2 (red) antibodies. Nuclei were stained with Hoechst (blue). Scale bar, 10 μm. Right: co-localization analysis of the fluorescence signals for the distance represented by white lines. See also Figures S5 and S6.

P53 level (Figure 9). Thus, this dually regulatory mechanism will exaggerate the complexity of USP7 in controlling the P53 stability and weaken the modulation specificity by targeting USP7. Given these seemingly contradictory roles of USP7 in modulating P53 signaling pathway, the biological consequences and its pharmacological effects of the polyQ-IRF modulation in cancer treatment remain to be explored in detail in future.

Direct sequestration of HDM2 for modulating P53 functionality

HDM2, a key negatively regulatory factor of P53, is overexpressed in many types of tumor cells,[55] whereas directly antagonizing HDM2 to activate P53 can be achieved through several strategies, such as inhibiting ubiquitin ligase activity of HDM2 or disrupting HDM2-P53 interaction. Targeting USP7 by the polyQ-IRF fusions indirectly affects the ubiquitination activity of HDM2 in cells, but they

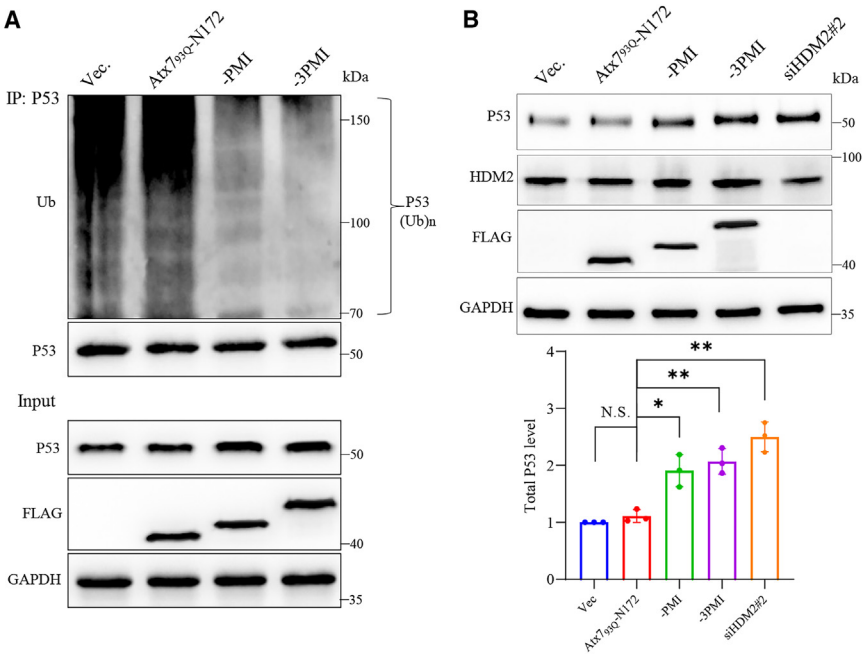

Figure 7. Sequestration of HDM2 by polyQ-PMI leads to enhancement of the P53 stability

(A) Detecting the ubiquitination level of P53 affected by polyQ-PMI fusions. HEK 293T cells were transfected with FLAG-tagged NLS-Atx7$_{93Q}$-N172 or its PMI/3PMI fusion. About 36 h post-transfection, the cells were treated with MG132 for 5 h. Subsequently, the cell lysates were subjected to immunoprecipitation using protein A + G agarose beads and anti-P53 antibody.

(B) Effect of the polyQ-PMI fusions on the P53 level. A549 cells were transfected with FLAG-tagged NLS-Atx7$_{93Q}$-N172 or its PMI/3PMI fusion, and 48 h post-transfection, the P53 levels in cell lysates were detected and analyzed. siHDM2 was set as a control. Vec., vector; Atx7$_{93Q}$-N172, with an NLS sequence; PMI, NLS-Atx7$_{93Q}$-N172-PMI; 3PMI, NLS-Atx7$_{93Q}$-N172-3PMI; siHDM2, siRNA targeting *HDM2*. Data are shown as mean ± SD ($n = 3$). *$p < 0.05$; **$p < 0.01$; N.S., no significance. See also Figures S7 and S8.

may have relatively low specificities toward P53. The polyQ-PMI fusions have been designed to specifically deplete the functional availability of HDM2 in cells by directly sequestrating HDM2 into aggregates.

Many small-molecule inhibitors are developed to interfere with the HDM2-P53 interaction for anticancer therapy.[56–59] However, they are likely to cause "off-target" toxicity due to their relatively low binding affinity or specificity.[60,61] The PMI peptide exhibits strong affinity and specificity for binding to HDM2,[42] effectively minimizing the off-target effects. The polyQ-PMI fusions can sequester HDM2 into aggregates (Figures 6, S5, and S6), reduce the availability of HDM2, and then cause the decrease of the P53 ubiquitination level in cells (Figures 7 and S7). This indicates that the ubiquitination function of HDM2 is abolished by polyQ-PMI sequestration, leading to suppressed ubiquitination and degradation capacities for P53. Consequently, expression of the P53 downstream genes is promoted at both mRNA and protein levels (Figure 8). This is reminiscent of the effect of RNA interference that activates P53 signaling by silencing HDM2 (Figure S8).

Potential therapeutic application of the polyQ-fusion technique

Small-molecule compounds targeting either USP7 or HDM2 have been demonstrated to modulate the P53 functionality in cancer cells.[62,63] However, despite their high efficacies, these compounds still face numerous challenges in clinical application, primarily including some issues with drug resistance, toxicity, off-target effects, and incomplete inhibition of the targeted pathway, which limit their widespread usage.[64,65] Short peptides are superior in inhibiting P53-HDM2 interaction due to their abilities to antagonize both HDM2 and HDMX with high affinities, while exhibiting relatively lower toxicities.[42,66,67] The PROTAC technique can be applied to induce targeted degradation of HDM2 by using either the PMI peptide or small-molecule inhibitor, which has been developed to modulate the P53 pathway and yield therapeutic gains.[59,68,69] The polyQ-PMI fusions we have designed to effectively sequester HDM2 significantly reduce its solubility and availability in cells. It is possible that the aggregates formed by polyQ-PMI can redistribute HDM2 in the nucleus and subsequently interfere with its nuclear function in ubiquitination of P53. Of note, formation of polyQ-PMI aggregates may also enhance the stability of the PMI peptide itself, preventing it from degradation by intracellular proteases.[70]

For engineered polyQ fusion proteins, it should be concerned that the off-target effects are important to treating efficacy. Although these fusion proteins are designed to specifically sequester the target proteins (enzymes) such as USP7 and HDM2, their aggregation properties may also lead to non-specific interactions with other non-target proteins, resulting in any potential off-target effects. Moreover, besides HDM2, USP7 may have multiple substrates such as PTEN and Axin; targeting USP7 can also interfere with the PI3K/AKT and Wnt/β-catenin signaling pathways,[48,71] which may cause unpredictable side effects. Therefore, minimizing the off-target effects is critical in the development of polyQ fusions.

It is obvious that polyQ proteins require a specific threshold of glutamine repeats to induce protein aggregation[72,73]; the shorter repeats are generally insufficient to induce substantial aggregation, whereas longer repeats facilitate the formation of aggregates, which can sequester other cellular components and subsequently disrupt their normal biological functions.[16,74] In this respect, optimization of the polyQ length is essential for achieving the desired polyQ fusion constructs. To some extent, mature protein aggregates are relatively inert or even protective to cells.[4,5] There is a possibility that the polyQ-fusion technique can minimize harmful impact on the

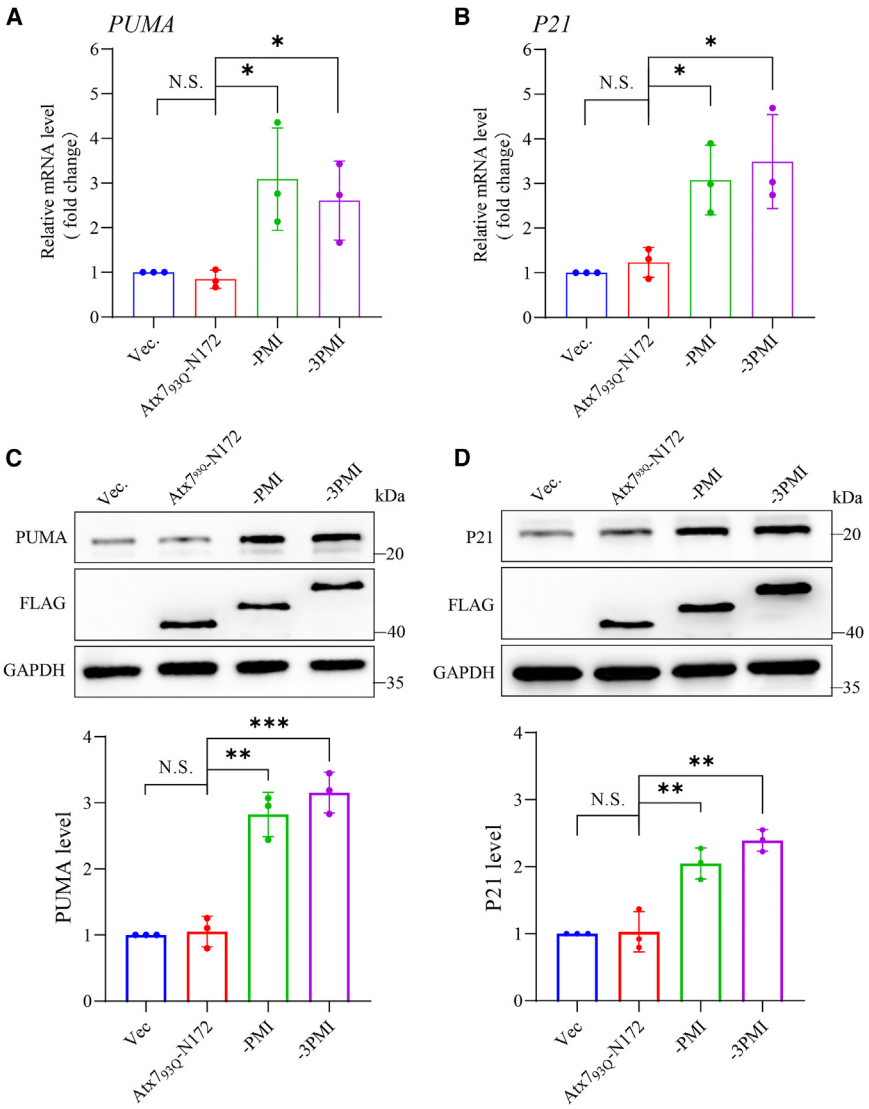

Figure 8. PolyQ-PMI fusions activate the P53 signaling pathway

(A and B) Detecting the mRNA levels of *PUMA* and *P21*. A549 cells were transfected with FLAG-tagged NLS-Atx7$_{93Q}$-N172 or its PMI/3PMI fusion, and after cultured for 48 h, the cells were lysed with TRIzol to extract RNA, then the mRNA levels of *PUMA* (A) and *P21* (B) were detected and analyzed.

(C and D) Detecting the protein levels of PUMA and P21. A549 cells were transfected with FLAG-tagged NLS-Atx7$_{93Q}$-N172 or its PMI/3PMI fusion, and after cultured for 48 h, the cells were lysed in RIPA buffer containing 8M urea, then the protein levels of PUMA (C) and P21 (D) were detected and analyzed. Vec., vector; Atx7$_{93Q}$-N172, with an NLS sequence; PMI, NLS-Atx7$_{93Q}$-N172-PMI; 3PMI, NLS-Atx7$_{93Q}$-N172-3PMI. Data are shown as mean ± SD (n = 3). *p < 0.05; **p < 0.01; ***p < 0.001; N.S., no significance. See also Figure S8.

overall physiological function of the cell by altering the functional status of cellular components rather than completely degrading them.

We have demonstrated that the designer polyQ fusions can modulate the P53 functionality by redistributing USP7 and/or HDM2 from their functional compartments. This polyQ fusion strategy can also extend to modulate other biological pathways or processes by targeting the key proteins (enzymes) for therapeutic purposes. Further research on polyQ fusions is required to investigate their potential cytotoxicity, drug delivery, off-target effects, and more importantly translation to clinical application.

Limitations of the study

In this study, we have successfully developed a polyQ-fusion technique to modulate the biological function of USP7/HDM2 and hence to enhance the P53 stability. This goal was just achieved in cell models, but it still lacked evident data in animal models, which limits our understanding of the system efficacy, pharmacokinetics, and potential immune responses *in vivo*. We also recognize that the abnormal accumulation of mutant P53 can have detrimental effects in P53-related diseases, but our system is not able to selectively increase the protein level of wild-type P53 without affecting the mutant forms. Notably, polyQ protein aggregation is closely associated with neurodegenerative diseases; overexpression of the polyQ fusions may inevitably cause unintended cytotoxicity, making it complicated in therapeutic application. Although we have designed several polyQ fusions that specifically sequester USP7 and HDM2, the off-target effects and aberrant interactions with other proteins may disrupt cellular function and homeostasis. Thus, it should be clarified whether the potential benefits of this novel approach outweigh the risks under certain conditions. In addition, the long-term effects of polyQ aggregates on cellular homeostasis and even overall organism, including their clearance mechanisms and potential immune responses, remain underexplored. Detailed research is needed to assess the therapeutic potential, efficacy, and safety of the polyQ-fusion technology in more complicated biological environments, with particular focus on minimizing cytotoxicity, improving targeting specificity, and evaluating its efficacy under more physiologically relevant and disease-specific conditions.

RESOURCE AVAILABILITY

Lead contact

Further information and requests for resources, reagents, and materials should be directed to and will be fulfilled by the lead contact, Hong-Yu Hu (hyhu@sibcb.ac.cn).

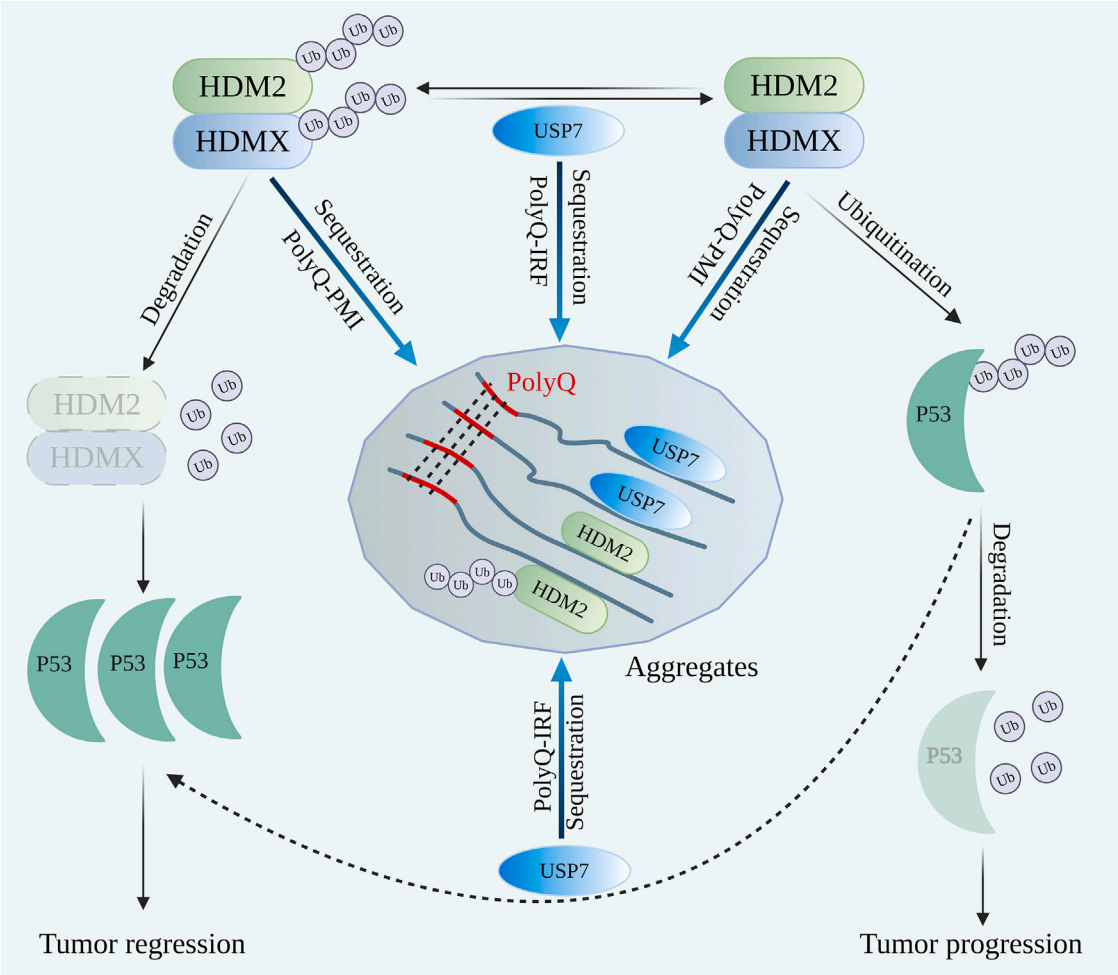

Figure 9. Schematic representation of the polyQ fusion proteins in modulating the USP7-HDM2-P53 pathway

PolyQ-IRF fusions can sequester USP7 into aggregates or inclusions via their fused IRF sequence and reduce the solubility and availability of USP7 in cells. This may attenuate deubiquitination of HDM2 and facilitate its degradation and thereby enhance the stability of P53. PolyQ-IRF can also sequester HDM2 into aggregates through the interaction of HDM2 with USP7, decreasing the functional availability of HDM2 and further increasing the stability of P53. On the other hand, because USP7 functions in deubiquitinating P53, excessive sequestration of USP7 may also interfere with the P53 deubiquitination process, which in turn reduces the P53 stability. Importantly, polyQ-PMI fusions directly sequester HDM2 into aggregates through its fused PMI sequence and thus reduce the solubility and availability of HDM2 in cells, which consequently reduces the ubiquitination level of P53 and enhances its stability and functionality.

Materials availability

All reagents generated in this study are available from the lead contact.

Data and code availability

- The DNA sequences for the constructs encoding the designer fusion proteins in this study have been deposited in the GenBank and are publicly available as of the date of publication. Accession numbers are listed in the key resources table.
- This paper does not report original code.
- The original unprocessed data are available in the *Mendeley Data* (https://doi.org/10.17632/hcrhrx7473.1). Any additional information required to reanalyze the data reported in this paper is available from the lead contact upon request.

ACKNOWLEDGMENTS

We would like to thank the Core Facility for Molecular Biology and the Core Facility for Cell Biology at CEMCS, CAS, for providing technical support in biochemical analysis and microscopic imaging. We also thank Prof. X. L. Mao at Guangzhou Medical University for kindly providing the plasmid encoding USP7. This work was supported by grants (31870764, 31670782) from the National Natural Science Foundation of China (to H.-Y.H.).

AUTHOR CONTRIBUTIONS

H.-Y.H., X.-L.Z., and H.-W.Y. conceived and designed the investigation. X.-L.Z., and H.-W.Y. performed the experiments and statistical analysis and analyzed the data. Y.-J.L., J.-Y.W., H.-T.D., and Y.-H.L. performed the experiments. L.-L.J. analyzed and stored the experimental data. X.-L.Z. and H.-Y.H. wrote and edited the manuscript.

DECLARATION OF INTERESTS

The authors have a patent **(2023112954096)** application and/or registration related to this work.

STAR★METHODS

Detailed methods are provided in the online version of this paper and include the following:

- KEY RESOURCES TABLE
- METHOD DETAILS
  - Plasmids, antibodies, and reagents
  - Cell culture, transfection, and Western blotting
  - Supernatant/pellet fractionation
  - Extraction of total protein
  - Immunoprecipitation (IP)
  - Ubiquitination assay
  - Immunofluorescence imaging
  - Quantitative RT-PCR assay
- QUANTIFICATION AND STATISTICAL ANALYSIS

SUPPLEMENTAL INFORMATION

Supplemental information can be found online at https://doi.org/10.1016/j.isci.2025.112025.

Received: July 3, 2024
Revised: November 5, 2024
Accepted: February 11, 2025
Published: February 13, 2025

REFERENCES

1. Housmans, J.A.J., Wu, G., Schymkowitz, J., and Rousseau, F. (2023). A guide to studying protein aggregation. FEBS J. *290*, 554–583. https://doi.org/10.1111/febs.16312.
2. Chiti, F., and Dobson, C.M. (2017). Protein Misfolding, Amyloid Formation, and Human Disease: A Summary of Progress Over the Last Decade. Annu. Rev. Biochem. *86*, 27–68. https://doi.org/10.1146/annurev-biochem-061516-045115.
3. Lieberman, A.P., Shakkottai, V.G., and Albin, R.L. (2019). Polyglutamine Repeats in Neurodegenerative Diseases. Annu. Rev. Pathol. *14*, 1–27. https://doi.org/10.1146/annurev-pathmechdis-012418-012857.
4. Arrasate, M., Mitra, S., Schweitzer, E.S., Segal, M.R., and Finkbeiner, S. (2004). Inclusion body formation reduces levels of mutant huntingtin and the risk of neuronal death. Nature *431*, 805–810. https://doi.org/10.1038/nature02998.
5. Saudou, F., Finkbeiner, S., Devys, D., and Greenberg, M.E. (1998). Huntingtin acts in the nucleus to induce apoptosis but death does not correlate with the formation of intranuclear inclusions. Cell *95*, 55–66. https://doi.org/10.1016/s0092-8674(00)81782-1.
6. Mahul-Mellier, A.L., Burtscher, J., Maharjan, N., Weerens, L., Croisier, M., Kuttler, F., Leleu, M., Knott, G.W., and Lashuel, H.A. (2020). The process of Lewy body formation, rather than simply α-synuclein fibrillization, is one of the major drivers of neurodegeneration. Proc. Natl. Acad. Sci. USA *117*, 4971–4982. https://doi.org/10.1073/pnas.1913904117.
7. Yang, H., Liu, S., He, W.T., Zhao, J., Jiang, L.L., and Hu, H.Y. (2015). Aggregation of Polyglutamine-expanded Ataxin 7 Protein Specifically Sequesters Ubiquitin-specific Protease 22 and Deteriorates Its Deubiquitinating Function in the Spt-Ada-Gcn5-Acetyltransferase (SAGA) Complex. J. Biol. Chem. *290*, 21996–22004. https://doi.org/10.1074/jbc.M114.631663.
8. Jiang, Y.J., Che, M.X., Yuan, J.Q., Xie, Y.Y., Yan, X.Z., and Hu, H.Y. (2011). Interaction with polyglutamine-expanded huntingtin alters cellular distribution and RNA processing of huntingtin yeast two-hybrid protein A (HYPA). J. Biol. Chem. *286*, 25236–25245. https://doi.org/10.1074/jbc.M110.216333.
9. Guo, X., Sun, X., Hu, D., Wang, Y.J., Fujioka, H., Vyas, R., Chakrapani, S., Joshi, A.U., Luo, Y., Mochly-Rosen, D., and Qi, X. (2016). VCP recruitment to mitochondria causes mitophagy impairment and neurodegeneration in models of Huntington's disease. Nat. Commun. *7*, 12646. https://doi.org/10.1038/ncomms12646.
10. Yang, H., Yue, H.W., He, W.T., Hong, J.Y., Jiang, L.L., and Hu, H.Y. (2018). PolyQ-expanded huntingtin and ataxin-3 sequester ubiquitin adaptors hHR23B and UBQLN2 into aggregates via conjugated ubiquitin. FASEB J. *32*, 2923–2933. https://doi.org/10.1096/fj.201700801RR.
11. Yue, H.W., Hong, J.Y., Zhang, S.X., Jiang, L.L., and Hu, H.Y. (2021). PolyQ-expanded proteins impair cellular proteostasis of ataxin-3 through sequestering the co-chaperone HSJ1 into aggregates. Sci. Rep. *11*, 7815. https://doi.org/10.1038/s41598-021-87382-w.
12. Zeng, L., Wang, B., Merillat, S.A., Minakawa, E.N., Perkins, M.D., Ramani, B., Tallaksen-Greene, S.J., Costa, M.d.C., Albin, R.L., and Paulson, H.L. (2015). Differential recruitment of UBQLN2 to nuclear inclusions in the polyglutamine diseases HD and SCA3. Neurobiol. Dis. *82*, 281–288. https://doi.org/10.1016/j.nbd.2015.06.017.
13. Jiang, L.L., Guan, W.L., Wang, J.Y., Zhang, S.X., and Hu, H.Y. (2022). RNA-assisted sequestration of RNA-binding proteins by cytoplasmic inclusions of the C-terminal 35-kDa fragment of TDP-43. J. Cell Sci. *135*, jcs259380. https://doi.org/10.1242/jcs.259380.
14. Guan, W.L., Jiang, L.L., Yin, X.F., and Hu, H.Y. (2023). PABPN1 aggregation is driven by Ala expansion and poly(A)-RNA binding, leading to CFIm25 sequestration that impairs alternative polyadenylation. J. Biol. Chem. *299*, 105019. https://doi.org/10.1016/j.jbc.2023.105019.
15. Hu, H.Y., and Liu, Y.J. (2022). Sequestration of cellular native factors by biomolecular assemblies: Physiological or pathological? Biochim. Biophys. Acta Mol. Cell Res. *1869*, 119360. https://doi.org/10.1016/j.bbamcr.2022.119360.
16. Yang, H., and Hu, H.Y. (2016). Sequestration of cellular interacting partners by protein aggregates: implication in a loss-of-function pathology. FEBS J. *283*, 3705–3717. https://doi.org/10.1111/febs.13722.
17. Orr, H.T., and Zoghbi, H.Y. (2007). Trinucleotide repeat disorders. Annu. Rev. Neurosci. *30*, 575–621. https://doi.org/10.1146/annurev.neuro.29.051605.113042.
18. Lee, J.T., and Gu, W. (2010). The multiple levels of regulation by p53 ubiquitination. Cell Death Differ. *17*, 86–92. https://doi.org/10.1038/cdd.2009.77.
19. Pellegrino, M., Mancini, F., Lucà, R., Coletti, A., Giacchè, N., Manni, I., Arisi, I., Florenzano, F., Teveroni, E., Buttarelli, M., et al. (2015). Targeting the MDM2/MDM4 interaction interface as a promising approach for p53 reactivation therapy. Cancer Res. *75*, 4560–4572. https://doi.org/10.1158/0008-5472.CAN-15-0439.
20. Sheng, Y., Saridakis, V., Sarkari, F., Duan, S., Wu, T., Arrowsmith, C.H., and Frappier, L. (2006). Molecular recognition of p53 and MDM2 by USP7/HAUSP. Nat. Struct. Mol. Biol. *13*, 285–291. https://doi.org/10.1038/nsmb1067.
21. Li, M., Brooks, C.L., Kon, N., and Gu, W. (2004). A dynamic role of HAUSP in the p53-Mdm2 pathway. Mol. Cell *13*, 879–886. https://doi.org/10.1016/s1097-2765(04)00157-1.
22. Kubbutat, M.H., Jones, S.N., and Vousden, K.H. (1997). Regulation of p53 stability by Mdm2. Nature *387*, 299–303. https://doi.org/10.1038/387299a0.
23. Brooks, C.L., Li, M., Hu, M., Shi, Y., and Gu, W. (2007). The p53–Mdm2–HAUSP complex is involved in p53 stabilization by HAUSP. Oncogene *26*, 7262–7266. https://doi.org/10.1038/sj.onc.1210531.
24. Dai, C., and Gu, W. (2010). p53 post-translational modification: deregulated in tumorigenesis. Trends Mol. Med. *16*, 528–536. https://doi.org/10.1016/j.molmed.2010.09.002.
25. Vassilev, L.T., Vu, B.T., Graves, B., Carvajal, D., Podlaski, F., Filipovic, Z., Kong, N., Kammlott, U., Lukacs, C., Klein, C., et al. (2004). In vivo activation of the p53 pathway by small-molecule antagonists of MDM2. Science *303*, 844–848. https://doi.org/10.1126/science.1092472.

26. Chauhan, D., Tian, Z., Nicholson, B., Kumar, K.G.S., Zhou, B., Carrasco, R., McDermott, J.L., Leach, C.A., Fulcinniti, M., Kodrasov, M.P., et al. (2012). A small molecule inhibitor of ubiquitin-specific protease-7 induces apoptosis in multiple myeloma cells and overcomes bortezomib resistance. Cancer Cell *22*, 345–358. https://doi.org/10.1016/j.ccr.2012.08.007.

27. Reverdy, C., Conrath, S., Lopez, R., Planquette, C., Atmanene, C., Collura, V., Harpon, J., Battaglia, V., Vivat, V., Sippl, W., and Colland, F. (2012). Discovery of specific inhibitors of human USP7/HAUSP deubiquitinating enzyme. Chem. Biol. *19*, 467–477. https://doi.org/10.1016/j.chembiol.2012.02.007.

28. Vicente, A.T.S., and Salvador, J.A.R. (2022). MDM2-Based Proteolysis-Targeting Chimeras (PROTACs): An Innovative Drug Strategy for Cancer Treatment. Int. J. Mol. Sci. *23*, 11068. https://doi.org/10.3390/ijms231911068.

29. Hu, M., Gu, L., Li, M., Jeffrey, P.D., Gu, W., and Shi, Y. (2006). Structural basis of competitive recognition of p53 and MDM2 by HAUSP/USP7: implications for the regulation of the p53-MDM2 pathway. PLoS Biol. *4*, e27. https://doi.org/10.1371/journal.pbio.0040027.

30. Chavoshi, S., Egorova, O., Lacdao, I.K., Farhadi, S., Sheng, Y., and Saridakis, V. (2016). Identification of Kaposi Sarcoma Herpesvirus (KSHV) vIRF1 Protein as a Novel Interaction Partner of Human Deubiquitinase USP7. J. Biol. Chem. *291*, 6281–6291. https://doi.org/10.1074/jbc.M115.710632.

31. Dai, X., Lu, L., Deng, S., Meng, J., Wan, C., Huang, J., Sun, Y., Hu, Y., Wu, B., Wu, G., et al. (2020). USP7 targeting modulates anti-tumor immune response by reprogramming Tumor-associated Macrophages in Lung Cancer. Theranostics *10*, 9332–9347. https://doi.org/10.7150/thno.47137.

32. Saha, G., Roy, S., Basu, M., and Ghosh, M.K. (2023). USP7 - a crucial regulator of cancer hallmarks. Biochim. Biophys. Acta Rev. Canc *1878*, 188903. https://doi.org/10.1016/j.bbcan.2023.188903.

33. Meulmeester, E., Maurice, M.M., Boutell, C., Teunisse, A.F.A.S., Ovaa, H., Abraham, T.E., Dirks, R.W., and Jochemsen, A.G. (2005). Loss of HAUSP-mediated deubiquitination contributes to DNA damage-induced destabilization of Hdmx and Hdm2. Mol. Cell *18*, 565–576. https://doi.org/10.1016/j.molcel.2005.04.024.

34. Al-Eidan, A., Wang, Y., Skipp, P., and Ewing, R.M. (2022). The USP7 protein interaction network and its roles in tumorigenesis. Genes Dis. *9*, 41–50. https://doi.org/10.1016/j.gendis.2020.10.004.

35. Zhang, T., Periz, G., Lu, Y.N., and Wang, J. (2020). USP7 regulates ALS-associated proteotoxicity and quality control through the NEDD4L-SMAD pathway. Proc. Natl. Acad. Sci. USA *117*, 28114–28125. https://doi.org/10.1073/pnas.2014349117.

36. Mehta, S., Campbell, H., Drummond, C.J., Li, K., Murray, K., Slatter, T., Bourdon, J.C., and Braithwaite, A.W. (2021). Adaptive homeostasis and the p53 isoform network. EMBO Rep. *22*, e53085. https://doi.org/10.15252/embr.202153085.

37. Pei, Y., Fu, J., Shi, Y., Zhang, M., Luo, G., Luo, X., Song, N., Mi, T., Yang, Y., Li, J., et al. (2022). Discovery of a Potent and Selective Degrader for USP7. Angew Chem. Int. Ed. Engl. *61*, e202204395. https://doi.org/10.1002/anie.202204395.

38. Sancar, A., Lindsey-Boltz, L.A., Unsal-Kaçmaz, K., and Linn, S. (2004). Molecular mechanisms of mammalian DNA repair and the DNA damage checkpoints. Annu. Rev. Biochem. *73*, 39–85. https://doi.org/10.1146/annurev.biochem.73.011303.073723.

39. Benchimol, S. (2001). p53-dependent pathways of apoptosis. Cell Death Differ. *8*, 1049–1051. https://doi.org/10.1038/sj.cdd.4400918.

40. Li, T., Kon, N., Jiang, L., Tan, M., Ludwig, T., Zhao, Y., Baer, R., and Gu, W. (2012). Tumor suppression in the absence of p53-mediated cell-cycle arrest, apoptosis, and senescence. Cell *149*, 1269–1283. https://doi.org/10.1016/j.cell.2012.04.026.

41. Koo, N., Sharma, A.K., and Narayan, S. (2022). Therapeutics Targeting p53-MDM2 Interaction to Induce Cancer Cell Death. Int. J. Mol. Sci. *23*, 5005. https://doi.org/10.3390/ijms23095005.

42. Li, C., Pazgier, M., Li, C., Yuan, W., Liu, M., Wei, G., Lu, W.Y., and Lu, W. (2010). Systematic mutational analysis of peptide inhibition of the p53-MDM2/MDMX interactions. J. Mol. Biol. *398*, 200–213. https://doi.org/10.1016/j.jmb.2010.03.005.

43. Pazgier, M., Liu, M., Zou, G., Yuan, W., Li, C., Li, C., Li, J., Monbo, J., Zella, D., Tarasov, S.G., and Lu, W. (2009). Structural basis for high-affinity peptide inhibition of p53 interactions with MDM2 and MDMX. Proc. Natl. Acad. Sci. USA *106*, 4665–4670. https://doi.org/10.1073/pnas.0900947106.

44. Karni-Schmidt, O., Lokshin, M., and Prives, C. (2016). The Roles of MDM2 and MDMX in Cancer. Annu. Rev. Pathol. *11*, 617–644. https://doi.org/10.1146/annurev-pathol-012414-040349.

45. Wang, H., Guo, M., Wei, H., and Chen, Y. (2023). Targeting p53 pathways: mechanisms, structures, and advances in therapy. Signal Transduct. Targeted Ther. *8*, 92. https://doi.org/10.1038/s41392-023-01347-1.

46. Qi, S.M., Cheng, G., Cheng, X.D., Xu, Z., Xu, B., Zhang, W.D., and Qin, J.J. (2020). Targeting USP7-Mediated Deubiquitination of MDM2/MDMX-p53 Pathway for Cancer Therapy: Are We There Yet? Front. Cell Dev. Biol. *8*, 233. https://doi.org/10.3389/fcell.2020.00233.

47. Pozhidaeva, A., Valles, G., Wang, F., Wu, J., Sterner, D.E., Nguyen, P., Weinstock, J., Kumar, K.G.S., Kanyo, J., Wright, D., and Bezsonova, I. (2017). USP7-Specific Inhibitors Target and Modify the Enzyme's Active Site via Distinct Chemical Mechanisms. Cell Chem. Biol. *24*, 1501–1512.e5. https://doi.org/10.1016/j.chembiol.2017.09.004.

48. Song, M.S., Salmena, L., Carracedo, A., Egia, A., Lo-Coco, F., Teruya-Feldstein, J., and Pandolfi, P.P. (2008). The deubiquitinylation and localization of PTEN are regulated by a HAUSP-PML network. Nature *455*, 813–817. https://doi.org/10.1038/nature07290.

49. Tavana, O., Li, D., Dai, C., Lopez, G., Banerjee, D., Kon, N., Chen, C., Califano, A., Yamashiro, D.J., Sun, H., and Gu, W. (2016). HAUSP deubiquitinates and stabilizes N-Myc in neuroblastoma. Nat. Med. *22*, 1180–1186. https://doi.org/10.1038/nm.4180.

50. Tavana, O., and Gu, W. (2017). Modulation of the p53/MDM2 interplay by HAUSP inhibitors. J. Mol. Cell Biol. *9*, 45–52. https://doi.org/10.1093/jmcb/mjw049.

51. Mitra, S., Tsvetkov, A.S., and Finkbeiner, S. (2009). Single neuron ubiquitin-proteasome dynamics accompanying inclusion body formation in huntington disease. J. Biol. Chem. *284*, 4398–4403. https://doi.org/10.1074/jbc.M806269200.

52. Liu, Y.J., Wang, J.Y., Zhang, X.L., Jiang, L.L., and Hu, H.Y. (2024). Ataxin-2 sequesters Raptor into aggregates and impairs cellular mTORC1 signaling. FEBS J. *291*, 1795–1812. https://doi.org/10.1111/febs.17081.

53. Wang, J.Y., Liu, Y.J., Zhang, X.L., Liu, Y.H., Jiang, L.L., and Hu, H.Y. (2024). PolyQ-expanded ataxin-2 aggregation impairs cellular processing-body homeostasis via sequestering the RNA helicase DDX6. J. Biol. Chem. *300*, 107413. https://doi.org/10.1016/j.jbc.2024.107413.

54. Li, M., Chen, D., Shiloh, A., Luo, J., Nikolaev, A.Y., Qin, J., and Gu, W. (2002). Deubiquitination of p53 by HAUSP is an important pathway for p53 stabilization. Nature *416*, 648–653. https://doi.org/10.1038/nature737.

55. Liu, Y., Wang, X., Wang, G., Yang, Y., Yuan, Y., and Ouyang, L. (2019). The past, present and future of potential small-molecule drugs targeting p53-MDM2/MDMX for cancer therapy. Eur. J. Med. Chem. *176*, 92–104. https://doi.org/10.1016/j.ejmech.2019.05.018.

56. Holzer, P., Masuya, K., Furet, P., Kallen, J., Valat-Stachyra, T., Ferretti, S., Berghausen, J., Bouisset-Leonard, M., Buschmann, N., Pissot-Soldermann, C., et al. (2015). Discovery of a Dihydroisoquinolinone Derivative (NVP-CGM097): A Highly Potent and Selective MDM2 Inhibitor Undergoing Phase 1 Clinical Trials in p53wt Tumors. J. Med. Chem. *58*, 6348–6358. https://doi.org/10.1021/acs.jmedchem.5b00810.

57. Ding, Q., Zhang, Z., Liu, J.J., Jiang, N., Zhang, J., Ross, T.M., Chu, X.J., Bartkovitz, D., Podlaski, F., Janson, C., et al. (2013). Discovery of RG7388, a potent and selective p53-MDM2 inhibitor in clinical development. J. Med. Chem. *56*, 5979–5983. https://doi.org/10.1021/jm400487c.

58. Canon, J., Osgood, T., Olson, S.H., Saiki, A.Y., Robertson, R., Yu, D., Eksterowicz, J., Ye, Q., Jin, L., Chen, A., et al. (2015). The MDM2 Inhibitor AMG 232 Demonstrates Robust Antitumor Efficacy and Potentiates the Activity of p53-Inducing Cytotoxic Agents. Mol. Cancer Therapeut. *14*, 649–658. https://doi.org/10.1158/1535-7163.MCT-14-0710.

59. Fang, Y., Liao, G., and Yu, B. (2020). Small-molecule MDM2/X inhibitors and PROTAC degraders for cancer therapy: advances and perspectives. Acta Pharm. Sin. B *10*, 1253–1278. https://doi.org/10.1016/j.apsb.2020.01.003.

60. Shangary, S., Qin, D., McEachern, D., Liu, M., Miller, R.S., Qiu, S., Nikolovska-Coleska, Z., Ding, K., Wang, G., Chen, J., et al. (2008). Temporal activation of p53 by a specific MDM2 inhibitor is selectively toxic to tumors and leads to complete tumor growth inhibition. Proc. Natl. Acad. Sci. USA *105*, 3933–3938. https://doi.org/10.1073/pnas.0708917105.

61. Shangary, S., and Wang, S. (2009). Small-molecule inhibitors of the MDM2-p53 protein-protein interaction to reactivate p53 function: a novel approach for cancer therapy. Annu. Rev. Pharmacol. Toxicol. *49*, 223–241. https://doi.org/10.1146/annurev.pharmtox.48.113006.094723.

62. Kategaya, L., Di Lello, P., Rougé, L., Pastor, R., Clark, K.R., Drummond, J., Kleinheinz, T., Lin, E., Upton, J.P., Prakash, S., et al. (2017). USP7 small-molecule inhibitors interfere with ubiquitin binding. Nature *550*, 534–538. https://doi.org/10.1038/nature24006.

63. Konopleva, M., Martinelli, G., Daver, N., Papayannidis, C., Wei, A., Higgins, B., Ott, M., Mascarenhas, J., and Andreeff, M. (2020). MDM2 inhibition: an important step forward in cancer therapy. Leukemia *34*, 2858–2874. https://doi.org/10.1038/s41375-020-0949-z.

64. Deng, J., Liang, L., Yi, H., Su, T., Yang, Z., Nie, L., and Liu, J. (2020). USP7 inhibition inhibits proliferation and induces megakaryocytic differentiation in MDS cells by upregulating gelsolin. Br. J. Haematol. *190*, 418–429. https://doi.org/10.1111/bjh.16549.

65. Whitebread, S., Dumotier, B., Armstrong, D., Fekete, A., Chen, S., Hartmann, A., Muller, P.Y., and Urban, L. (2016). Secondary pharmacology: screening and interpretation of off-target activities - focus on translation. Drug Discov. Today *21*, 1232–1242. https://doi.org/10.1016/j.drudis.2016.04.021.

66. Phan, J., Li, Z., Kasprzak, A., Li, B., Sebti, S., Guida, W., Schönbrunn, E., and Chen, J. (2010). Structure-based design of high affinity peptides inhibiting the interaction of p53 with MDM2 and MDMX. J. Biol. Chem. *285*, 2174–2183. https://doi.org/10.1074/jbc.M109.073056.

67. Brown, C.J., Quah, S.T., Jong, J., Goh, A.M., Chiam, P.C., Khoo, K.H., Choong, M.L., Lee, M.A., Yurlova, L., Zolghadr, K., et al. (2013). Stapled peptides with improved potency and specificity that activate p53. ACS Chem. Biol. *8*, 506–512. https://doi.org/10.1021/cb3005148.

68. Chen, S., Li, X., Li, Y., Yuan, X., Geng, C., Gao, S., Li, J., Ma, B., Wang, Z., Lu, W., and Hu, H.G. (2022). Design of stapled peptide-based PROTACs for MDM2/MDMX atypical degradation and tumor suppression. Theranostics *12*, 6665–6681. https://doi.org/10.7150/thno.75444.

69. Ma, B., Feng, H., Feng, C., Liu, Y., Zhang, H., Wang, J., Wang, W., He, P., and Niu, F. (2022). Kill Two Birds with One Stone: A Multifunctional Dual-Targeting Protein Drug to Overcome Imatinib Resistance in Philadelphia Chromosome-Positive Leukemia. Adv. Sci. *9*, e2104850. https://doi.org/10.1002/advs.202104850.

70. Liu, M., Pazgier, M., Li, C., Yuan, W., Li, C., and Lu, W. (2010). A left-handed solution to peptide inhibition of the p53-MDM2 interaction. Angew Chem. Int. Ed. Engl. *49*, 3649–3652. https://doi.org/10.1002/anie.201000329.

71. Ji, L., Lu, B., Zamponi, R., Charlat, O., Aversa, R., Yang, Z., Sigoillot, F., Zhu, X., Hu, T., Reece-Hoyes, J.S., et al. (2019). USP7 inhibits Wnt/beta-catenin signaling through promoting stabilization of Axin. Nat. Commun. *10*, 4184. https://doi.org/10.1038/s41467-019-12143-3.

72. Brignull, H.R., Moore, F.E., Tang, S.J., and Morimoto, R.I. (2006). Polyglutamine proteins at the pathogenic threshold display neuron-specific aggregation in a pan-neuronal Caenorhabditis elegans model. J. Neurosci. *26*, 7597–7606. https://doi.org/10.1523/jneurosci.0990-06.2006.

73. Barton, S., Jacak, R., Khare, S.D., Ding, F., and Dokholyan, N.V. (2007). The length dependence of the polyQ-mediated protein aggregation. J. Biol. Chem. *282*, 25487–25492. https://doi.org/10.1074/jbc.M701600200.

74. Hands, S.L., and Wyttenbach, A. (2010). Neurotoxic protein oligomerisation associated with polyglutamine diseases. Acta Neuropathol. *120*, 419–437. https://doi.org/10.1007/s00401-010-0703-0.

STAR★METHODS

KEY RESOURCES TABLE

REAGENT or RESOURCE	SOURCE	IDENTIFIER
Antibodies		
Mouse monoclonal anti-FLAG	Sigma-Aldrich	Cat# F1804; RRID: AB_262044
Mouse monoclonal anti-HA	Sigma-Aldrich	Cat# H3663; RRID: AB_262051
Rabbit polyclonal anti-USP7	Novus	Cat# NB100-513; RRID: AB_2257070
Rabbit monoclonal anti-HDM2	Abcam	Cat# ab259265; RRID: AB_2920616
Rabbit monoclonal anti-HDM2	Cell Signaling Technology	Cat# 86934S; RRID: AB_2784534
Rabbit polyclonal anti-PUMA	Proteintech	Cat# 55120-1-AP; RRID: AB_10859944
Rabbit polyclonal anti-Ub	Proteintech	Cat# 10201-2-AP; RRID: AB_671515
Mouse monoclonal anti-P53	Santa Cruz	Cat# sc-126; RRID: AB_628082
Mouse monoclonal anti-GAPDH	Proteintech	Cat# 60004-1-Ig; RRID: AB_2107436
Rabbit polyclonal anti-P21	Proteintech	Cat# 10355-1-AP; RRID: AB_2077682
Peroxidase AffiniPure Goat Anti-Mouse IgG (H+L)	Jackson ImmunoResearch Laboratories	Cat# 115-035-003; RRID: AB_10015289
Peroxidase AffiniPure Goat Anti-Rabbit IgG (H+L)	Jackson ImmunoResearch Laboratories	Cat# 111-001-003; RRID: AB_2337910
FITC IgG Fluorescein-Conjugated AffiniPure Goat Anti-Rabbit IgG(H+L)	ZsBIO	Cat# ZF-0311; RRID: AB_2571576
TRITC IgG Fluorescein-Conjugated AffiniPure Goat Anti-Rabbit IgG(H+L)	ZsBIO	Cat# ZF-0316; RRID: AB_2728778
FITC IgG Fluorescein-Conjugated AffiniPure Goat Anti-Mouse IgG(H+L)	ZsBIO	Cat# ZF-0312; RRID: AB_2716306
TRITC IgG Fluorescein-Conjugated AffiniPure Goat Anti-Mouse IgG(H+L)	ZsBIO	Cat# ZF-0313; RRID: AB_2571577
Bacterial and virus strains		
TOP10	TIANGEN	Cat# CB104
Chemicals, peptides, and recombinant proteins		
Cocktail protease inhibitor	Roche	Cat# 04693132001
Hoechst 33342	Sigma-Aldrich	Cat# B2261
MG132	Cell Signaling Technology	Cat# 2194S
N-ethylmaleimide	TargetMol	Cat# T3088
Critical commercial assays		
ECL detection reagent	Thermo Fisher Scientific	Cat# 32106
Anti-FLAG-Tag Mouse Antibody (Agarose Conjugated)	Abmart	Cat# M20018
4 x Reverse Transcription Master Mix	EZBioscience	Cat# A0010
Hieff qPCR SYBR Green Master Mix	Yeasen Biotech	Cat# 11201ES08*
PolyJet reagent	SignaGen	Cat# SL100688
Lipofectamine™ 3000	Thermo Fisher Scientific	Cat# L3000075
NucleoBond Xtra Midi EF, Midi kit	MACHEREY-NAGEL	Cat# 740420.50
Deposited data		
Raw and analyzed data	This paper; Mendeley Data	https://doi.org/10.17632/hcrhrx7473.1
NLS-Htt_{18Q}-N171	GenBank	PP861293
NLS-Htt_{18Q}-N171-IRF	GenBank	PP861294
NLS-Htt_{18Q}-N171-3IRF	GenBank	PP861295
NLS-Htt_{100Q}-N171	GenBank	PP861296
NLS-Htt_{100Q}-N171-IRF	GenBank	PP861297

(*Continued on next page*)

Continued		
REAGENT or RESOURCE	SOURCE	IDENTIFIER
NLS-Htt_{100Q}-N171-3IRF	GenBank	PP861298
NLS-$Atx7_{10Q}$-N172	GenBank	PP861299
NLS-$Atx7_{10Q}$-N172-IRF	GenBank	PP861300
NLS-$Atx7_{10Q}$-N172-3IRF	GenBank	PP861301
NLS-$Atx7_{10Q}$-N172-PMI	GenBank	PP861302
NLS-$Atx7_{10Q}$-N172-3PMI	GenBank	PP861303
NLS-$Atx7_{93Q}$-N172	GenBank	PP861304
NLS-$Atx7_{93Q}$-N172-IRF	GenBank	PP861305
NLS-$Atx7_{93Q}$-N172-3IRF	GenBank	PP861306
NLS-$Atx7_{93Q}$-N172-PMI	GenBank	PP861307
NLS-$Atx7_{93Q}$-N172-3PMI	GenBank	PP861308
Experimental models: Cell lines		
A549 cell	Cell Bank, Chinese Academy of Sciences	N/A
HEK 293T cell	Cell Bank, Chinese Academy of Sciences	N/A
Oligonucleotides		
Primers for PCR/qPCR, see Table S2	This paper	N/A
siRNA targeting sequence: see Table S3	This paper	N/A
Recombinant DNA		
Plasmids, see Table S1	This paper	N/A
Software and algorithms		
SageCapture	Sage Creation Science	http://www.sagecreation.com.cn/en/
GraphPad Prism	GraphPad Software	https://www.graphpad.com/
ImageJ	ImageJ	https://imagej.net/
Leica TCS SP8 WLL	Leica	https://www.leicamicrosystems.com/
LAS X	Leica	https://www.leicamicrosystems.com/

METHOD DETAILS

Plasmids, antibodies, and reagents

The DNA sequences for encoding NLS-fused Htt_{18Q}-N171 (residues 1-171), Htt_{100Q}-N171, $Atax7_{10Q}$-N172 (residues 1-172) and $Atx7_{93Q}$-N172 were cloned in the FLAG-pcDNA3.1 vector.[11] The cDNAs encoding NLS-Htt_{18Q}-N171 or NLS-Htt_{100Q}-N171 fused with a peptide (IRF/3IRF) in the C-terminus were inserted into the FLAG-pcDNA3.1 vector via EcoR I/Xba I sites. The cDNAs encoding NLS-$Atx7_{10Q}$-N172 or NLS-$Atx7_{93Q}$-N172 fused with a peptide (IRF/2IRF/3IRF, PMI/3PMI) in the C-terminus were inserted into the FLAG-pcDNA3.1 vector via EcoR I/Xba I sites. The DNA sequences for USP7 and HDM2 were cloned into the HA-pcDNA3.1 vector using BamH I/Xba I sites. All the DNA sequences were verified by DNA sequencing (Table S1), and the PCR primers used in this study were listed in nucleotide sequences (Table S2).

The anti-FLAG and anti-HA antibodies were purchased from Sigma, anti-USP7 was from Novus, and anti-MDM2 was from Cell Signaling Technology or Abcam. The anti-P21, anti-PUMA and anti-GAPDH antibodies were from Proteintech; anti-P53 were purchased from Santa Cruz. All secondary antibodies were from Jackson ImmunoResearch Laboratories. MG132 was purchased from Cell Signaling Technology.

Cell culture, transfection, and Western blotting

HEK 293T cells and A549 cells, obtained from the Cell Bank of the Chinese Academy of Sciences (Shanghai), were cultured in Dulbecco's Modified Eagle's Medium (HyClone) supplemented with 10% fetal bovine serum (Gibco) and penicillin-streptomycin. The culture conditions were maintained at 37°C in a humidified atmosphere with 5% CO_2. Plasmid transfections were conducted using PolyJet reagent (SignaGen) according to the manufacturer's protocol, while transfection of siRNA (Table S3) was performed with Lipofectamine 3000 (Invitrogen). For protein analysis, the cell lysates were processed through SDS-PAGE and subsequently transferred onto PVDF membranes (Millipore). The blots were sectioned as necessary before antibody incubation. Detection of the specific proteins was achieved using appropriate primary and secondary antibodies, followed by visualization with an ECL detection kit

(ThermoFisher Scientific). Quantitative analysis of the protein bands was conducted using integral grayscale values, recorded via *Sage Capture* software (http://www.sagecreation.com.cn/en/).

Supernatant/pellet fractionation

Supernatant/pellet (S/P) fractionation was conducted as described previously.[13,52] Approximately 48 hrs post transfection, HEK 293T or A549 cells were collected and lysed in 90 μL of the RIPA buffer (50 mM Tris, pH7.5, 150 mM NaCl, 1 mM EDTA, 1% NP-40, and protease inhibitor cocktail (Roche)) on ice for 30 min. The lysates were then centrifuged at 13,000 rpm for 15 min at 4°C. Subsequently, 80 μL of the supernatant was mixed with 20 μL of the 5 x loading buffer (8% SDS). The pellet was thoroughly washed three times with the RIPA buffer at 4°C and resuspended in 40 μL of the 5 x loading buffer (8% SDS). Equal volumes of both supernatant and pellet fractions were analyzed by SDS-PAGE and Western blotting.

Extraction of total protein

Approximately 48 hrs post transfection, the cultured cells were harvested and lysed in 100 μL of the RIPA buffer supplemented with 8 M urea, ensuring thorough dissolution of all aggregated forms of protein. This was followed by addition of 100 μL of 2 x loading buffer (containing 2% SDS and 8 M urea) to the lysates. Subsequently, the protein samples obtained were boiled for denaturation and then processed for SDS-PAGE and Western blotting analysis.

Immunoprecipitation (IP)

Immunoprecipitation was performed according to a previously outlined protocol.[7] About 48 hrs following transfection, the HEK 293T cells were harvested and harvested with the RIPA buffer (50 mM Tris, pH7.5, 150 mM NaCl, 1mM EDTA, 1% NP-40 and protease inhibitor cocktail (Roche)). Post lysis, the cell lysates were centrifuged at 13,000 rpm for 20 min at 4°C. Following incubation for 4 hrs, the anti-FLAG beads (Abmart) were washed three times with the RIPA buffer before boiling in 40 μL of the 2 x loading buffer (4% SDS). The protein eluates from these beads were then subjected to immunoblotting analysis.

Ubiquitination assay

About 36 hrs following transfection, cells were incubated with an indicated dose of MG-132 (Cell Signaling Technology) for 5 hrs to promote accumulation of the polyubiquitinated proteins prior to collection. Subsequently, the cell lysis was performed using an SDS lysis buffer (50 mM Tris, pH6.8; 1% SDS, 10% glycerol, protease inhibitor cocktail (ThermoFisher)). Post boiling for 10 min, the lysates were diluted tenfold in an IP Lysis buffer (50 mM Tris, pH8.0, 150 mM NaCl, 1% Triton X-100), which was further enriched with 15 mM NEM (Target MOL) and additional protease inhibitors. These diluted lysates were then subjected to immunoprecipitation using specific antibodies, followed by probing with an anti-ubiquitin antibody for detection. Finally, to identify other specified proteins, 10% of the input was analyzed via immunoblotting.

Immunofluorescence imaging

For immunofluorescence imaging, the cells cultured on glass coverslips were processed approximately 48 hrs post transfection or at the specified culture duration. Initially, the cells were washed with a phosphate-buffered solution (PBS) (10 mM Na_2HPO_4, 1.8 mM KH_2PO_4, 140 mM NaCl, 2.7 mM KCl, pH7.3) and then fixed using 4% paraformaldehyde for 15 min. After three washes with the PBS buffer, the cells were permeabilized with 0.1% Triton X-100 and blocked in a solution containing 5% bovine serum albumin in the PBS buffer for 1 hr at room temperature. The cells were then incubated overnight at 4°C with specific primary antibodies. Following primary antibody incubation, the cells were washed with the PBS buffer and then incubated with either fluorescein isothiocyanate (FITC)-conjugated or tetramethyl rhodamine isothiocyanate (TRITC)-conjugated secondary antibodies (Jackson ImmunoResearch Laboratories). Nuclei were stained with Hoechst (ThermoFisher Scientific). The imaging was performed using a Leica TCS SP8 WLL confocal microscope (Leica Microsystems), and the images were captured using *LAS X* software (https://www.leicamicrosystems.com/) and presented without modification.

Quantitative RT-PCR assay

Total RNA was extracted from cultured HEK 293T cells using TRIzol reagent (Life Technologies) following the manufacturer's instructions. The cDNA synthesis was performed using 4 x Reverse Transcription Master Mix (EZBioscience) with 2 μg of total RNA from each sample. Quantitative real-time PCR (qPCR) was conducted using Hieff qPCR SYBR Green Master Mix (Yeasen Biotech) on a LightCycler96 PCR system (Roche). The qPCR reactions were set up in a total volume of 20 μL, comprising 10 μL of SYBR Green Master Mix, 2 μL of cDNA template, and 0.5 mM of each primer (Table S2). The fold changes of mRNA expression were quantified using the $2^{-\Delta Ct}$ algorithm, normalized against the *GAPDH* expression. This assay was replicated in three independent experiments to ensure reliability of the results.

QUANTIFICATION AND STATISTICAL ANALYSIS

Quantitative analysis of the Western blots was conducted using *ImageJ* software (https://imagej.net/). The integral grayscale values of the indicated protein bands were normalized against those of respective controls. Data were derived from a minimum of three independent experiments and are presented as Mean ± SD. Statistical analyses were performed using *GraphPad Prism* 7.0 (https://www.graphpad.com/) with the student's t-test. Statistical significance was established at $p < 0.05$, where the p-values were denoted in graphs as * ($p < 0.05$), ** ($p < 0.01$), *** ($p < 0.001$), or N.S. (no significance).